PHILOSOPHICAL TRANSACTIONS OF THE ROYAL SOCIETY A MATHEMATICAL, PHYSICAL & ENGINEERING SCIENCES

Mixed Finite Element Substructure-Subdomain Methods for the Dynamical Analysis of Coupled Fluid-Solid Interaction Problems

Jing-Tang Xing, W. G. Price and Q. H. Du

Phil. Trans. R. Soc. Lond. A 1996 **354**, 259-295
doi: 10.1098/rsta.1996.0009

Mixed finite element substructure–subdomain methods for the dynamical analysis of coupled fluid–solid interaction problems

By Jing-Tang Xing[1,2], W. G. Price[2] and Q. H. Du[3]

[1]*Solid Mechanics Research Center, Beijing University of Aeronautics and Astronautics, Beijing 100083, People's Republic of China*
[2]*Department of Ship Science, University of Southampton, Highfield, Southampton SO9 5NH, UK*
[3]*Department of Engineering Mechanics, Tsinghua University, Beijing 100084, People's Republic of China*

Contents

Phil. Trans. R. Soc. Lond. A (1996) **354**, 259–295
Printed in Great Britain

Based on a variational method adopting the dynamic pressure in the fluid and the acceleration in the solid as arguments in the functional, several substructure–subdomain methods are developed to describe the dynamical behaviour of fluid–structure systems excited externally. Formulations are presented of a displacement consistency model and a hybrid displacement model for the solid structure, a pressure equilibrium model for the fluid and a mixed substructure–subdomain model for the fluid–structure interacting system.

These substructure–subdomain methods make the mixed finite-element approaches developed to analyse fluid–solid interactions more effective and efficient especially in calculating solutions to large complex engineering problems. This is achieved through the suitable selection of mode vectors to reduce the number of degrees of freedom accepted in the finite-element method to a manageable size without reducing significantly the accuracy of solution; by synthesis of the equations modelling the dynamic interactions and by developing techniques to eliminate mathematical difficulties occurring in the matrix formulations. By these means, consistent and unifying theoretical models are developed to describe the dynamical behaviour of the solid, fluid and their interactions which are in forms adaptable for solution on a personal computer. This is demonstrated by analysing a wide selection of fluid–structure (e.g. dam–water system excited by earthquake or explosion) and air–structure (e.g. structural-borne noise in a fuselage) interacting systems using purposely written computer software.

1. Introduction

In a previous paper (Xing & Price 1991), we developed a mixed finite-element approach to describe the linear dynamics of coupled fluid–structure interactions. This approach is based on a variational principle in which the variables of acceleration in the elastic solid and pressure in the fluid are adopted as the arguments in the functional. The method was successfully demonstrated by analysing a wide selection of fluid–structure interaction problems of practical interest. However, experience shows that for very large complicated fluid–structure interaction problems possibly involving many tens of thousands degrees of freedom, computational difficulties arise (e.g. storage, time, etc.). These problems can be overcome by a frontal attack using a large and/or more sophisticated computer or more suitably, and certainly more satisfying, by developing new methods and techniques to make the solution process more effective and computationally more efficient.

Such reasoning is not new for, in the past, substructure methods or component mode synthesis methods were developed to derive solutions describing the dynamical behaviour of large engineering structures. The potential of the method, originally developed by Hunn (1955), was realized by Hurty (1960) and over the years it has been

PHILOSOPHICAL TRANSACTIONS OF THE ROYAL SOCIETY A MATHEMATICAL, PHYSICAL & ENGINEERING SCIENCES

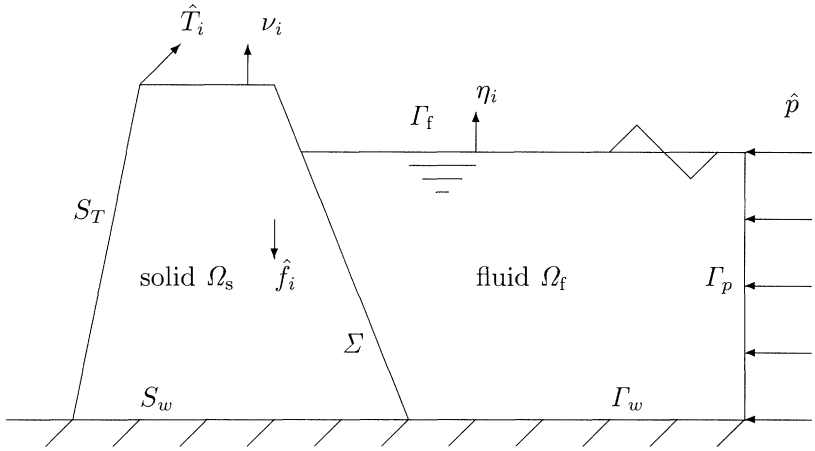

Figure 1. A fluid–solid interaction system excited by an explosion wave $\hat{p}$ in water.

further developed and refined to tackle large dynamics problems (see, for example, Hurty 1965; Hou 1969; Craig & Bampton 1968; Rubin 1975; Craig & Chang 1977; MacNeal 1977; Wang 1979). Based on the variational principles of elastodynamics, Xing (1981) and Xing & Zheng (1983) applied the substructure method to the dynamic analysis of dry structures. From suitably formulated substructure models they studied the convergence of the methods and derived a rule on which mode reduction could be undertaken in a reasoned and logical way. Applications and extensions of the substructure approach have been made by Unruch (1979) and Xing (1984, 1986*a*, *b*) to study fluid–structure interaction problems. This paper continues such studies with the development of an unified substructure–subdomain method incorporating the mixed finite-element approach discussed previously (see, for example, Xing & Price 1991). To explain the main features of the proposed approach, let us consider the fluid–structure system shown in figure 1. Here the elastic structure (i.e. a dam) of domain Ω_s and surface S $(= S_T \cup S_w \cup \Sigma)$ is in contact at the interface Σ with fluid occupying the domain Ω_f and is enclosed by the surface Γ $(= \Gamma_w \cup \Gamma_f \cup \Gamma_p \cup \Sigma)$. A wave exists on the surface Γ_f and $\hat{p}$ denotes a prescribed boundary pressure caused by an explosion (say). The quantities η_i and ν_i denote unit vectors along the outer normals to Γ and S respectively, $\hat{T}_i$ represents a prescribed traction on S_T and $\hat{f}_i$ represents a body force vector. The development of the substructure–subdomain method to derive solutions to this fluid–structure interaction problem, relies on the following three steps:

(i) The whole fluid–structure system under examination is divided into several smaller subsystems. For example, figure 2 illustrates a simple four-subsystem idealization to model the elastic dam–fluid configuration shown in figure 1. The dam is divided into two substructures Sub_1 and Sub_2. Sub_1 represents a dry solid substructure with no contact with the fluid while Sub_2 represents a solid substructure adjacent to the fluid. Similarly, the fluid is divided into two subdomains Sub_3 and Sub_4. Sub_3 represents a fluid subdomain in contact with the solid whereas Sub_4 represents a fluid subdomain with no boundary common to the solid. A line $(- \bullet -)$ indicates an interface between substructures and/or subdomains. Naturally, the number of subsystems can be greatly increased but this increases the detailed definition of the problem rather than modifying the basic modelling procedures.

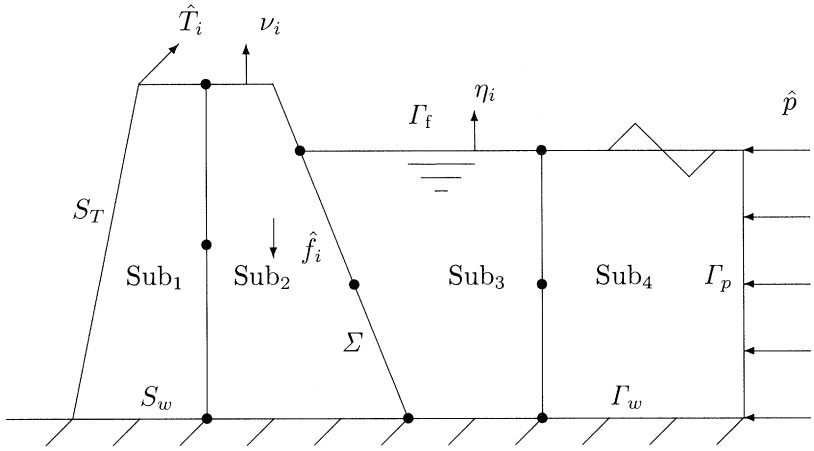

Figure 2. The dynamical system in figure 1 divided into four substructure–subdomains. Sub_1 and Sub_2 are the substructures of the solid. Sub_3 and Sub_4 are the subdomains of the fluid. The lines $-\bullet-$ represent the interfaces between substructures, subdomains and substructure–subdomains.

(ii) Finite-element analysis of substructure–subdomain. A finite-element analysis is applied to each substructure or subdomain to derive data describing their dynamic characteristics. These data form the basis for the construction of the solution to the fluid–structure interaction problem.

(iii) Synthesis of substructure–subdomain. By developing suitable theoretical approaches and techniques, the data contributing significantly to the dynamics of the system can be deduced and, in a systematic way, synthesized to obtain an approximate solution describing the dynamics of the whole system.

The substructure–subdomain method is a development combining the Rayleigh–Ritz method and a finite-element analysis. It takes advantages of the positive aspects of both methods but avoids their shortcomings. It divides a large vibrational problem into smaller problems of a size more easily handled, and a solution to the larger problem is obtained by suitably combining the solutions of the smaller problems. In many ways, this reflects the same thinking as described by Bishop & Johnson (1979) in developing and describing the application of receptance theory to solve vibrational problems.

Based on variational formulations this paper describes the development of a substructure–subdomain method to analyse the dynamical behaviour of large complex fluid–structure interaction problems. Solid, fluid and mixed models describing the substructures and subdomains are presented as well as descriptions of mode reduction techniques and the synthesis of substructure and/or subdomain equations. To illustrate the flexibility and applicability of the proposed approach a wide ranging selection of dynamic problems are described and discussed involving fluid–structure (e.g. dam–water system excited by earthquake or explosion) and air–structure (e.g. structural-borne noise) interactions.

2. Governing equations and variational formulation

In order to assess the dynamical behaviour of the typical fluid–structure interaction system shown in figure 1, we need to model mathematically the dynamic

characteristics of the flexible structure within the solid domain Ω_s, the fluid with free surface in fluid domain Ω_f and the interacting mechanism at the fluid–structure interface Σ. The linear equations describing the fluid–structure interaction can be expressed in standard tensor notation as follows.

(*a*) *Solid domain*

(i) *Dynamic equation*

$$\sigma_{ij,j} + \hat{f}_i = \rho_s w_i, \qquad (x_i, t) \in \Omega_s \times (t_1, t_2). \tag{2.1}$$

(ii) *Strain-displacement*

$$e_{ij} = \tfrac{1}{2}(u_{i,j} + u_{j,i}), \qquad (x_i, t) \in \Omega_s \times (t_1, t_2). \tag{2.2}$$

(iii) *Constitutive equation*

$$\sigma_{ij} = a_{ijkl} e_{kl}, \qquad (x_i, t) \in \Omega_s \times (t_1, t_2), \tag{2.3}$$

and, assuming linearity, we have

$$\left.\begin{aligned} v_i &= u_{i,t}, \\ w_i &= v_{i,t}, \\ d_{ij} = e_{ij,t} &= \tfrac{1}{2}(v_{i,j} + v_{j,i}), \qquad (x_i, t) \in \Omega_s \times (t_1, t_2), \end{aligned}\right\} \tag{2.4}$$

where $u_{i,j} = \partial u_i / \partial x_j$, $u_{i,t} = \partial u_i / \partial t$, etc.

(iv) *Boundary conditions*

$$\text{acceleration:} \quad w_i = \hat{w}_i, \qquad (x_i, t) \in S_w \times [t_1, t_2], \tag{2.5}$$

$$\text{traction:} \quad \sigma_{ij}\nu_j = \hat{T}_i, \qquad (x_i, t) \in S_T \times [t_1, t_2]. \tag{2.6}$$

(*b*) *Fluid domain*

(i) *Dynamic equation*

$$p_{,tt} = c^2 p_{,ii}, \qquad (x_i, t) \in \Omega_f \times (t_1, t_2). \tag{2.7}$$

(ii) *Free surface*

$$p_{,i}\eta_i = -p_{,tt}/g, \qquad (x_i, t) \in \Gamma_f \times [t_1, t_2], \tag{2.8}$$

and these equations are complemented by boundary conditions on the

$$\text{pressure:} \quad p = \hat{p}, \qquad (x_i, t) \in \Gamma_p \times [t_1, t_2], \tag{2.9}$$

$$\text{acceleration:} \quad p_{,i}\eta_i = -\rho_f \hat{w}_i \eta_i, \qquad (x_i, t) \in \Gamma_w \times [t_1, t_2], \tag{2.10}$$

where

$$p_{,tt} = \frac{\partial^2 p}{\partial t^2}, \qquad p_{,ii} = \frac{\partial^2 p}{\partial x_1^2} + \frac{\partial^2 p}{\partial x_2^2} + \frac{\partial^2 p}{\partial x_3^2},$$

etc., and subscripts i, j, k and l ($l = 1, 2, 3$) obey the summation convention.

(c) Fluid–structure interface

At the fluid–structure interface boundary Σ, the equations describing the dynamics at this interface are

$$\text{normal acceleration:} \quad p_{,i}\eta_i = -\rho_{\mathrm{f}} w_i \eta_i, \qquad (x_i, t) \in \Sigma \times [t_1, t_2], \tag{2.11}$$

$$\text{pressure:} \quad \sigma_{ij}\nu_j = p\eta_i, \qquad (x_i, t) \in \Sigma \times [t_1, t_2]. \tag{2.12}$$

On the basis of these equations, Xing & Price (1991) developed a variational principle taking the dynamic pressure $p(x_i, t)$ in the fluid and the acceleration $w_i(x_j, t)$ in the solid as arguments in the functional. That is, a variational formulation is derived by considering the functional,

$$\begin{aligned} H[p, w_i] = \int_{t_1}^{t_2} \Big\{ \int_{\Omega_{\mathrm{s}}} [\tfrac{1}{2}\rho_{\mathrm{s}} w_i w_i - \tfrac{1}{2} a_{ijkl} d_{ij} d_{kl} - \hat{f}_i w_i] \, \mathrm{d}\Omega - \int_{S_T} \hat{T}_i w_i \, \mathrm{d}S \Big\} \mathrm{d}t \\ + \int_{t_1}^{t_2} \Big\{ \int_{\Omega_{\mathrm{f}}} \left[\frac{1}{2\rho_{\mathrm{f}} c^2} p_{,t} p_{,t} - \frac{1}{2\rho_{\mathrm{f}}} p_{,i} p_{,i} \right] \mathrm{d}\Omega + \int_{\Gamma_{\mathrm{f}}} \frac{1}{2\rho_{\mathrm{f}} g} p_{,t} p_{,t} \, \mathrm{d}\Gamma \\ - \int_{\Gamma_w} p \hat{w}_i \eta_i \, \mathrm{d}\Gamma \Big\} \mathrm{d}t - \int_{t_1}^{t_2} \int_{\Sigma} p w_i \eta_i \, \mathrm{d}S \mathrm{d}t. \end{aligned} \tag{2.13}$$

This functional is subject to the constraints expressed in equations (2.2), (2.4), (2.5) and (2.9) as well as the imposed initial t_1 and final t_2 time variational conditions:

$$\delta v_i(t_1) = 0 = \delta v_i(t_2), \qquad x_i \in \hat{\Omega}_{\mathrm{s}}, \tag{2.14}$$

$$\delta p_i(t_1) = 0 = \delta p_i(t_2), \qquad x_i \in \hat{\Omega}_{\mathrm{f}}. \tag{2.15}$$

The stationary conditions of the functional given in equation (2.13) are described in equations (2.1), (2.6), (2.7), (2.8), (2.10), (2.11) and (2.12).

3. Variational formulations for substructure–subdomain methods

In the process of discretizing the solid and fluid media into finite-elements, it was found advantageous in the development of the previously proposed mixed finite-element method by the authors, to express the functional H in terms of global arguments $\boldsymbol{p}$ and $\ddot{\boldsymbol{U}}$. (Here we substitute the variables $\ddot{\boldsymbol{U}}$ and $\dot{\boldsymbol{U}}$ for $\boldsymbol{W}$ and $\tilde{\boldsymbol{W}}$ used previously, because they now have a more direct physical representation.) Under this slight change of notation, the functional described in equation (2.13) can be expressed in the following matrix form:

$$\begin{aligned} H_{\mathrm{sf}}[\boldsymbol{p}, \ddot{\boldsymbol{U}}] = \int_{t_1}^{t_2} (\tfrac{1}{2}\ddot{\boldsymbol{U}}^{\mathrm{T}} \boldsymbol{M} \ddot{\boldsymbol{U}} - \tfrac{1}{2}\dot{\boldsymbol{U}}^{\mathrm{T}} \boldsymbol{K} \dot{\boldsymbol{U}} - \ddot{\boldsymbol{U}}^{\mathrm{T}} \hat{\boldsymbol{F}}) \, \mathrm{d}t \\ + \int_{t_1}^{t_2} (\tfrac{1}{2}\dot{\boldsymbol{p}}^{\mathrm{T}} \boldsymbol{m} \dot{\boldsymbol{p}} - \tfrac{1}{2}\boldsymbol{p}^{\mathrm{T}} \boldsymbol{k} \boldsymbol{p} - \boldsymbol{p}^{\mathrm{T}} \hat{\boldsymbol{u}}) \, \mathrm{d}t - \int_{t_1}^{t_2} \boldsymbol{p}^{\mathrm{T}} \boldsymbol{R} \ddot{\boldsymbol{U}} \, \mathrm{d}t, \end{aligned} \tag{3.1}$$

where $\boldsymbol{M}$ and $\boldsymbol{K}$ represent respectively the finite-element mass and stiffness matrices of the dry structure; $\boldsymbol{m}$ and $\boldsymbol{k}$ represent the finite-element matrices of the fluid domain and $\boldsymbol{R}$ denotes the fluid–structure interaction matrix.

For the separate dynamic problems of structure with no fluid and fluid with no structure, it follows from the previous result that the two functionals describing these

situations are

$$H_{\mathrm{s}}[\ddot{\boldsymbol{U}}] = \int_{t_1}^{t_2} (\tfrac{1}{2}\ddot{\boldsymbol{U}}^{\mathrm{T}}\boldsymbol{M}\ddot{\boldsymbol{U}} - \tfrac{1}{2}\dot{\boldsymbol{U}}^{\mathrm{T}}\boldsymbol{K}\dot{\boldsymbol{U}} - \ddot{\boldsymbol{U}}^{\mathrm{T}}\hat{\boldsymbol{F}})\,\mathrm{d}t \tag{3.2}$$

for the structure, and

$$H_{\mathrm{f}}[\boldsymbol{p}] = \int_{t_1}^{t_2} (\tfrac{1}{2}\dot{\boldsymbol{p}}^{\mathrm{T}}\boldsymbol{m}\dot{\boldsymbol{p}} - \tfrac{1}{2}\boldsymbol{p}^{\mathrm{T}}\boldsymbol{k}\boldsymbol{p} - \boldsymbol{p}^{\mathrm{T}}\hat{\ddot{\boldsymbol{u}}})\,\mathrm{d}t \tag{3.3}$$

for the fluid only.

If the solid and the fluid are divided into $\mathrm{Sub_s}$ substructures and $\mathrm{Sub_f}$ subdomains, respectively, and the coupling interfaces between the fluid domains and the solid substructures are denoted by Σ_{sf}, then the functionals in equations (3.1)–(3.3) can be rewritten in summation forms corresponding to the substructures and subdomains as follows:

$$\begin{aligned} H_{\mathrm{sf}}[\boldsymbol{p}, \ddot{\boldsymbol{U}}] = {} & \sum_{\alpha=1}^{\mathrm{Sub_s}} \int_{t_1}^{t_2} (\tfrac{1}{2}\ddot{\boldsymbol{U}}^{\mathrm{T}}\boldsymbol{M}\ddot{\boldsymbol{U}} - \tfrac{1}{2}\dot{\boldsymbol{U}}^{\mathrm{T}}\boldsymbol{K}\dot{\boldsymbol{U}} - \ddot{\boldsymbol{U}}^{\mathrm{T}}\hat{\boldsymbol{F}})^{(\alpha)}\,\mathrm{d}t \\ & + \sum_{\beta=1}^{\mathrm{Sub_f}} \int_{t_1}^{t_2} (\tfrac{1}{2}\dot{\boldsymbol{p}}^{\mathrm{T}}\boldsymbol{m}\dot{\boldsymbol{p}} - \tfrac{1}{2}\boldsymbol{p}^{\mathrm{T}}\boldsymbol{k}\boldsymbol{p} - \boldsymbol{p}^{\mathrm{T}}\hat{\ddot{\boldsymbol{u}}})^{(\beta)}\,\mathrm{d}t \\ & - \sum_{\theta=1}^{\Sigma_{\mathrm{sf}}} \int_{t_1}^{t_2} (\boldsymbol{p}^{\mathrm{T}}\boldsymbol{R}\ddot{\boldsymbol{U}})^{(\theta)}\,\mathrm{d}t, \end{aligned} \tag{3.4}$$

$$H_{\mathrm{s}}[\ddot{\boldsymbol{U}}] = \sum_{\alpha=1}^{\mathrm{Sub_s}} \int_{t_1}^{t_2} (\tfrac{1}{2}\ddot{\boldsymbol{U}}^{\mathrm{T}}\boldsymbol{M}\ddot{\boldsymbol{U}} - \tfrac{1}{2}\dot{\boldsymbol{U}}^{\mathrm{T}}\boldsymbol{K}\dot{\boldsymbol{U}} - \ddot{\boldsymbol{U}}^{\mathrm{T}}\hat{\boldsymbol{F}})^{(\alpha)}\,\mathrm{d}t, \tag{3.5}$$

and

$$H_{\mathrm{f}}[\boldsymbol{p}] = \sum_{\beta=1}^{\mathrm{Sub_f}} \int_{t_1}^{t_2} (\tfrac{1}{2}\dot{\boldsymbol{p}}^{\mathrm{T}}\boldsymbol{m}\dot{\boldsymbol{p}} - \tfrac{1}{2}\boldsymbol{p}^{\mathrm{T}}\boldsymbol{k}\boldsymbol{p} - \boldsymbol{p}^{\mathrm{T}}\hat{\ddot{\boldsymbol{u}}})^{(\beta)}\,\mathrm{d}t. \tag{3.6}$$

Here the superscripts (α), (β) and (θ) represent the number of substructures admitted to describe the solid, the number of subdomains chosen to represent the fluid and the number of coupling interfaces, respectively. The functions to be integrated in each bracketed term are associated with the corresponding superscripts.

The variational descriptions in equations (3.4), (3.5) and (3.6) form the basis of the following discussion and it is shown that they allow a logical approach on which to develop mixed finite-element substructure–subdomain methods for the dynamical analysis of coupled fluid–structure interaction problems.

4. Displacement consistency model for solid substructure

Based on the functional described in equation (3.5), a consistent displacement model describing the dynamical behaviour of a solid substructure can be constructed. In this displacement based finite-element model, the displacement (or acceleration) at each node between two adjacent substructures must be equal, but equilibrium between two adjacent interface forces is not required in advance. Here lies the key to the manner of selection of suitable mode vectors. That is, they are suitably chosen

(i) to guarantee the consistency of displacement on interfaces and (ii) to construct a complete subspace.

Taking the variation of the functional (3.5), we obtain the result

$$\delta H_{\mathrm{s}}[\ddot{\boldsymbol{U}}] = \sum_{\alpha=1}^{\mathrm{Sub_s}} \int_{t_1}^{t_2} (\delta \ddot{\boldsymbol{U}}^{\mathrm{T}} \boldsymbol{M} \ddot{\boldsymbol{U}} - \delta \dot{\boldsymbol{U}}^{\mathrm{T}} \boldsymbol{K} \dot{\boldsymbol{U}} - \delta \ddot{\boldsymbol{U}}^{\mathrm{T}} \hat{\boldsymbol{F}})^{(\alpha)} \, \mathrm{d}t$$

$$= \sum_{\alpha=1}^{\mathrm{Sub_s}} \int_{t_1}^{t_2} \delta \ddot{\boldsymbol{U}}^{\mathrm{T}} (\boldsymbol{M} \ddot{\boldsymbol{U}} + \boldsymbol{K} \boldsymbol{U} - \hat{\boldsymbol{F}})^{(\alpha)} \, \mathrm{d}t. \tag{4.1}$$

Because of the independence of $\delta \ddot{\boldsymbol{U}}$ and by using the variation $\delta H_{\mathrm{s}} = 0$, we find that the equation describing the dynamical characteristics associated with a finite-element can be rewritten in a substructure equation form as follows:

$$\begin{bmatrix} M^{ii} & M^{ij} \\ M^{ji} & M^{jj} \end{bmatrix}^{(\alpha)} \begin{bmatrix} \ddot{U}^i \\ \ddot{U}^j \end{bmatrix}^{(\alpha)} + \begin{bmatrix} K^{ii} & K^{ij} \\ K^{ji} & K^{jj} \end{bmatrix}^{(\alpha)} \begin{bmatrix} U^i \\ U^j \end{bmatrix}^{(\alpha)} = \begin{bmatrix} \hat{F}^i \\ \hat{F}^j \end{bmatrix}^{(\alpha)} + \begin{bmatrix} 0 \\ F^j \end{bmatrix}^{(\alpha)}, \tag{4.2}$$

$$\sum_{\alpha=1}^{\mathrm{Sub_s}} F^{j(\alpha)} = 0. \tag{4.3}$$

In these equations, the superscript i represents the internal degrees of freedom of a substructure, the superscript j represents the degrees of freedom on the interface of two adjacent substructures and F^j denotes the interface force on the interface of a substructure. Here, no summation convention is used involving superscripts i and j.

For each substructure, it is assumed that the displacement can be decomposed into the two parts, namely U^i and U^j, satisfying the relation

$$\begin{bmatrix} U^i \\ U^j \end{bmatrix} = \begin{bmatrix} U_1^i \\ 0 \end{bmatrix} + \begin{bmatrix} U_0^i \\ U^j \end{bmatrix}. \tag{4.4}$$

The second component in this expression satisfies a relation defined by the equation,

$$\begin{bmatrix} K^{ii} & K^{ij} \\ K^{ji} & K^{jj} \end{bmatrix} \begin{bmatrix} U_0^i \\ U^j \end{bmatrix} = \begin{bmatrix} 0 \\ F_0^j \end{bmatrix}, \tag{4.5}$$

whereas the first component satisfies another relation defined by the equation,

$$\begin{bmatrix} M^{ii} & M^{ij} \\ M^{ji} & M^{jj} \end{bmatrix} \begin{bmatrix} \ddot{U}_1^i \\ 0 \end{bmatrix} + \begin{bmatrix} K^{ii} & K^{ij} \\ K^{ji} & K^{jj} \end{bmatrix} \begin{bmatrix} U_1^i \\ 0 \end{bmatrix}$$

$$= \begin{bmatrix} \hat{F}^i \\ \hat{F}^j \end{bmatrix} + \begin{bmatrix} 0 \\ F_1^j \end{bmatrix} - \begin{bmatrix} M^{ii} & M^{ij} \\ M^{ji} & M^{jj} \end{bmatrix} \begin{bmatrix} \ddot{U}_0^i \\ \ddot{U}^j \end{bmatrix}, \tag{4.6}$$

where $F^j = F_0^j + F_1^j$. It is observed that equation (4.5) provides a *quasi-static* relationship between U_0^i, U^j and its corresponding interface force component F_0^j in the sense that inertia forces are neglected. By the superposition principle, these inertia forces reappear in equation (4.6) as corrections to the solution U_1^i. From equation (4.5), we obtain the result

$$U_0^i = -(K^{ii})^{-1} K^{ij} U^j \tag{4.7}$$

and hence

$$\begin{bmatrix} U_0^i \\ U^j \end{bmatrix} = \begin{bmatrix} -(K^{ii})^{-1}K^{ij} \\ I^{jj} \end{bmatrix} U^j = \begin{bmatrix} X^{ij} \\ I^{jj} \end{bmatrix} U^j, \tag{4.8}$$

where I^{jj} is a unit matrix and $X^{ij} = -(K^{ii})^{-1}K^{ij}$ denotes a submatrix of the mode vector. The substitution of equation (4.8) into equation (4.6) gives

$$M^{ii}\ddot{U}_1^i + K^{ii}U_1^i = \hat{F}^i + [M^{ii}(K^{ii})^{-1}K^{ij} - M^{ij}]\ddot{U}^j, \tag{4.9}$$

allowing equations (4.8) and (4.9) to be used to define the set of mode vectors applicable to a consistent displacement model for the solid substructure.

In the previous formulation, the submatrix K^{ii} should be non-singular. If it is not so, the inverse of the submatrix K^{ii} will not exist but this difficulty can be overcome by a frequency shift method which is described later.

(*a*) *Sets of mode vectors*

(i) *Consistent displacement modes between interfaces*

Based on equations (4.5) and (4.8), consistent displacement modes between interfaces can now be defined by the equation,

$$\begin{bmatrix} K^{ii} & K^{ij} \\ K^{ji} & K^{jj} \end{bmatrix} \begin{bmatrix} X^{ij} \\ I^{jj} \end{bmatrix} = \begin{bmatrix} 0 \\ F_0^{jj} \end{bmatrix}. \tag{4.10}$$

The collection of such displacement modes between interfaces is given by

$$\boldsymbol{X} = \begin{bmatrix} X^{ij} \\ I^{jj} \end{bmatrix} = \begin{bmatrix} -(K^{ii})^{-1}K^{ij} \\ I^{jj} \end{bmatrix}. \tag{4.11}$$

Physically, these modes represent the static configuration of the substructure on which a unit displacement is successively imposed to each degree of freedom along the interface, with all other degrees of freedom along the interface held fixed.

(ii) *Normalized modes of a fixed interface substructure*

Based on equation (4.9), the normalized modes of a fixed interface substructure are the normalized natural shapes of vibration with the interfaces of the substructure held fixed. These mode vectors can be solved through the eigenvalue equation describing the natural vibration of the substructure corresponding to equation (4.9). That is

$$(K^{ii} - \omega_s^2 M^{ii})\phi_s^i = 0, \tag{4.12}$$

$$\Phi^{i\mathrm{T}} M^{ii} \Phi^i = I^{ii}, \qquad \Phi^{i\mathrm{T}} K^{ii} \Phi^i = \Lambda, \tag{4.13}$$

where Φ^i is the matrix of normalized modes in which the sth column vector is the eigenvector ϕ_s^i, and the diagonal matrix $\Lambda = \mathrm{diag}(\omega_s^2)$ defined by the square of the natural frequency ω_s of the substructure. By means of mode transformation, we can write

$$U_1^i = \Phi^i Q \tag{4.14}$$

and by using equation (4.9) the generalized coordinate vector associated with natural vibrations is given by

$$Q = -\Omega^2[\Lambda - \Omega^2 I]^{-1}(\Lambda^{-1}\Phi^{i\mathrm{T}}K^{ij} - \Phi^{i\mathrm{T}}M^{ij})U^j, \tag{4.15}$$

where $\hat{\boldsymbol{F}} = 0$ in equation (4.1).

In order to describe the contribution of the sth mode of the substructure to the structural mode having frequency Ω, it is necessary to define the following factors.

Frequency factor

$$q_{s\omega} = -\frac{\Omega^2}{\omega_s^2 - \Omega^2}, \tag{4.16}$$

with resonance occurring at $\omega_s = \Omega$.

Vibration shape factor

$$q_{s\phi} = \phi_s^{i\mathrm{T}}(\omega_s^{-2}K^{ij} - M^{ij})U^j. \tag{4.17}$$

Mode factor

$$q_s = -\frac{\Omega^2}{\omega_s^2 - \Omega^2}\phi_s^{i\mathrm{T}}(\omega_s^{-2}K^{ij} - M^{ij})U^j, \tag{4.18}$$

which represents the sth element of the generalized coordinate vector Q. This factor is influenced by both frequency and vibration shape factors.

By combining the collection of mode vectors $\boldsymbol{X}$ and $\boldsymbol{\Phi}^i$, we can express the motion of the substructure as

$$\boldsymbol{U} = \boldsymbol{X}U^j + \boldsymbol{\Phi}Q, \tag{4.19}$$

where the base vectors of the substructure motion space are the consistent displacement modes $\boldsymbol{X}$ defined in equation (4.11) and the normalized natural modes of the substructure with fixed interface

$$\boldsymbol{\Phi} = \begin{bmatrix} \Phi^i \\ 0 \end{bmatrix}. \tag{4.20}$$

The corresponding generalized coordinate vectors are the interface displacement U^j for the base vector $\boldsymbol{X}$ and the generalized coordinate Q for the normalized natural mode vectors. Evidently, the base vectors in this collection are complete and independent of each other, satisfying the following orthogonal relation

$$\boldsymbol{X}^{\mathrm{T}}\boldsymbol{K}\boldsymbol{\Phi} = \begin{bmatrix} -K^{ji}(K^{ii})^{-1} & I^{jj} \end{bmatrix} \begin{bmatrix} K^{ii} & K^{ij} \\ K^{ji} & K^{jj} \end{bmatrix} \begin{bmatrix} \Phi^i \\ 0 \end{bmatrix} = 0. \tag{4.21}$$

This selection of mode base vectors guarantees the consistency of displacement between two adjacent interfaces, but they also describe fully the configuration of the motions of the substructure.

(*b*) *Rule and method for mode reduction*

In simple terms, the basic rule applied to mode reduction relies on the consistency of displacement between substructure interfaces, the retention of substructure modes producing major contributions to the global structure mode and the neglect (hence reduction) of those which influence very little the overall result, so that a good approximation to the global mode is obtained. Generally, the consistent displacement modes should be retained and reductions sought in the normalized modes of substructures with fixed interfaces. From equation (4.19) the contributions of normalized modes to the displacement $\boldsymbol{U}$ of the substructure are determined by the product of $\boldsymbol{\Phi}$ and Q. Because each column in $\boldsymbol{\Phi}$ is normalized by the same normalizing factor, the contribution of each column in $\boldsymbol{\Phi}$ to the displacement $\boldsymbol{U}$ can be regarded as *equal*. The quantity of each element in Q represents the contribution of the corresponding

PHILOSOPHICAL TRANSACTIONS OF THE ROYAL SOCIETY A MATHEMATICAL, PHYSICAL & ENGINEERING SCIENCES

normalized mode of the substructure to the displacement $\boldsymbol{U}$. For example the sth element $q_s = q_{s\omega} q_{s\phi}$ of the generalized coordinate vector Q represents the contribution of the sth normalized mode, which is the sth column of the normalized mode matrix $\boldsymbol{\Phi}$, to the displacement of the substructure. The quantity q_s is dependent on frequency ω_s and vibration shape ϕ_s, which clearly illustrates an inadequacy in any reduction rule depending on frequency only. Let us examine the implications of such a reduction rule.

(i) *Frequency reduction and its influence*

The relation between the absolute value of the frequency factor $q_{s\omega}$ in equation (4.16) and the frequency ratio ω_s/Ω is shown in figure 3. This curve can be discussed by dividing the frequency domain into three separate regions as follows.

(*a*) In the vicinity of a resonance, i.e. $\omega_s \approx \Omega$, the absolute value of $q_{s\omega}$ is very large implying that modes with frequencies ω_s close to Ω should be retained.

(*b*) For $\omega_s \gg \Omega$, then

$$q_{s\omega} = -\frac{\Omega^2}{\omega_s^2}\left(1 + \frac{\Omega^2}{\omega_s^2} + \dots\right) \approx -\frac{\Omega^2}{\omega_s^2} \longrightarrow 0, \tag{4.22}$$

indicating that modes with frequencies ω_s much higher than Ω can be neglected from the point of view of frequency reduction.

(*c*) For $\omega_s \ll \Omega$, then

$$q_{s\omega} = 1 + \frac{\omega_s^2}{\Omega^2} + \dots \approx 1, \tag{4.23}$$

indicating that the frequency contribution factor associated with sufficiently low frequency modes of the substructure to the high frequency modes of the global structure is close to unity.

To summarize these results, the rule of reduction based on frequency only retains modes with natural frequencies close to the global frequency Ω and to neglect those modes with natural frequencies far from this frequency. Because characteristics of the global structure in the low frequency region are usually needed in engineering studies, modes with frequencies (2 or 3 times say) higher than the highest frequency Ω are commonly neglected in this type of analysis.

The effect of frequency reduction to the approximate solution can now be examined. For example, it follows from equations (4.2), (4.8), (4.11) and (4.15) that the equation describing the interface force on the substructure is given by

$$\begin{aligned} F^j &= \{(K^{jj} - \Omega^2 M^{jj}) - (K^{ji} - \Omega^2 M^{ji})\Phi^i(\Lambda - \Omega^2 I)^{-1}\Phi^{i\mathrm{T}}(K^{ij} - \Omega^2 M^{ij})\}U^j \\ &= \kappa^{jj} U^j, \end{aligned} \tag{4.24}$$

where the dynamical rigidity of a substructure interface is expressed as

$$\kappa^{jj} = (K^{jj} - \Omega^2 M^{jj}) - (K^{ji} - \Omega^2 M^{ji})\Phi^i(\Lambda - \Omega^2 I)^{-1}\Phi^{i\mathrm{T}}(K^{ij} - \Omega^2 M^{ij}). \tag{4.25}$$

In this relation, the factor $(\Lambda - \Omega^2 I)^{-1}$ is positive definite for $\omega_s^2 > \Omega^2$ and negative definite for $\omega_s^2 < \Omega^2$. Therefore, the neglect of high frequency modes causes a hardening (or stiffening) of the substructure interfaces. The resulting computation of frequency in the low frequency regime associated with the dynamical characteristics of the structure by this mode synthesis method produces higher estimates than the values calculated by the corresponding finite-element method. Alternatively, the neglect of low frequency modes causes a softening (or an increasing of flexibility) of the substructure interfaces and the reverse trend to the one previously described occurs.

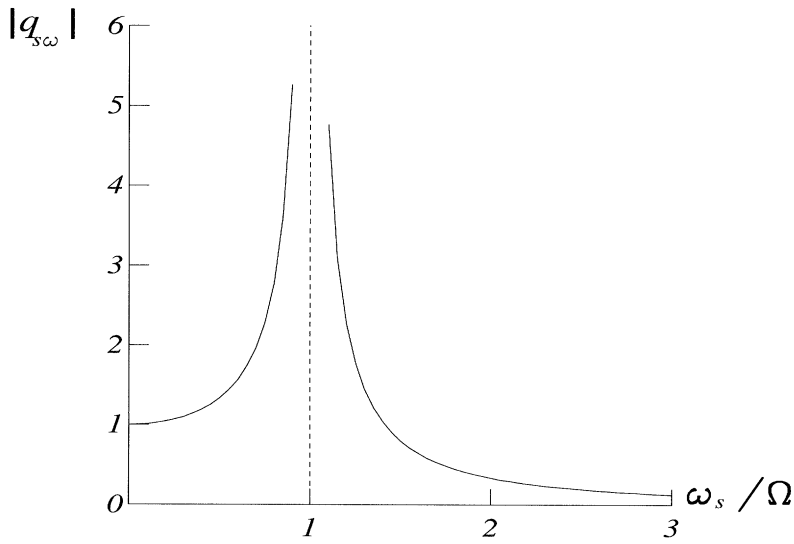

Figure 3. The curve of absolute value of frequency contribution factor $q_{s\omega}$ versus frequency ratio ω_s/Ω.

(ii) *The reduction depending on the vibration shape factor*

Although, in most cases, the important modes are retained through application of the frequency reduction rule, it is not infallible when dealing with a complex structure. In applying only a frequency dependent reduction rule, important modes may be missed and some unimportant modes may instead be inefficiently retained. These short comings may be overcome by developing a reduction procedure dependent on the vibration shape factor. Although vibration shape factors are unknown before the final synthesis, many of them can be assigned to a zero value because of symmetry considerations. In principle, a symmetric structure can be divided into substructures without destroying its symmetry. A symmetric mode of a substructure provides zero contribution to each antisymmetric mode of the structure and vice versa. Therefore symmetric and antisymmetric modes can be synthesized separately. In this way, the degrees of freedom, including those on interfaces, can be reduced more efficiently.

(*c*) *Synthesis of substructure equations*

Let $\boldsymbol{\Phi}_k^{(\alpha)}$ and $Q_k^{(\alpha)}$ denote respectively the remaining normalized modes of substructure (α) and the corresponding generalized coordinates. It follows from equation (4.19) that the motion of this substructure can be expressed as

$$\boldsymbol{U}^{(\alpha)} = [\boldsymbol{X}^{(\alpha)} \quad \boldsymbol{\Phi}_k^{(\alpha)}] \begin{bmatrix} U^{j(\alpha)} \\ Q_k^{(\alpha)} \end{bmatrix}, \tag{4.26}$$

or simply by

$$\boldsymbol{U}^{(\alpha)} = \tilde{\boldsymbol{\Phi}}^{(\alpha)} \tilde{\boldsymbol{Q}}^{(\alpha)}. \tag{4.27}$$

The substitution of equation (4.27) into equation (3.5) gives

$$H_{\mathrm{s}} = \sum_{\alpha=1}^{\mathrm{Sub_s}} \int_{t_1}^{t_2} (\tfrac{1}{2}\ddot{\tilde{\boldsymbol{Q}}}^{\mathrm{T}} \tilde{\boldsymbol{M}} \ddot{\tilde{\boldsymbol{Q}}} - \tfrac{1}{2}\dot{\tilde{\boldsymbol{Q}}}^{\mathrm{T}} \tilde{\boldsymbol{K}} \dot{\tilde{\boldsymbol{Q}}} - \ddot{\tilde{\boldsymbol{Q}}}^{\mathrm{T}} \tilde{\boldsymbol{F}})^{(\alpha)} \, \mathrm{d}t, \tag{4.28}$$

and through variation of this equation in conjunction with equations (4.21) and (4.13), the dynamical equation after synthesis may be cast into the form

$$\bar{\boldsymbol{M}} \ddot{\bar{\boldsymbol{Q}}} + \bar{\boldsymbol{K}} \bar{\boldsymbol{Q}} = \bar{\boldsymbol{F}}. \tag{4.29}$$

Here,

$$\left.\begin{aligned} &\tilde{\boldsymbol{Q}}^{(\alpha)} = \boldsymbol{T}^{(\alpha)} \bar{\boldsymbol{Q}}, \quad \bar{M} = \sum_{\alpha=1}^{\mathrm{Sub_s}} \boldsymbol{T}^{(\alpha)\mathrm{T}} \tilde{\boldsymbol{M}}^{(\alpha)} \boldsymbol{T}^{(\alpha)}, \quad \bar{\boldsymbol{K}} = \sum_{\alpha=1}^{\mathrm{Sub_s}} \boldsymbol{T}^{(\alpha)\mathrm{T}} \tilde{\boldsymbol{K}}^{(\alpha)} \boldsymbol{T}^{(\alpha)}, \\ &\bar{\boldsymbol{F}} = \sum_{\alpha=1}^{\mathrm{Sub_s}} \boldsymbol{T}^{(\alpha)\mathrm{T}} \tilde{F}^{(\alpha)}, \quad \tilde{\boldsymbol{M}}^{(\alpha)} = \begin{bmatrix} \boldsymbol{X}^{(\alpha)\mathrm{T}} \boldsymbol{M}^{(\alpha)} \boldsymbol{X}^{(\alpha)} & \boldsymbol{X}^{(\alpha)\mathrm{T}} \boldsymbol{M}^{(\alpha)} \boldsymbol{\Phi}_k^{(\alpha)} \\ \boldsymbol{\Phi}_k^{(\alpha)\mathrm{T}} \boldsymbol{M}^{(\alpha)} \boldsymbol{X}^{(\alpha)} & \boldsymbol{I}_k^{(\alpha)} \end{bmatrix}, \\ &\tilde{\boldsymbol{K}}^{(\alpha)} = \begin{bmatrix} \boldsymbol{X}^{(\alpha)\mathrm{T}} \boldsymbol{K}^{(\alpha)} \boldsymbol{X}^{(\alpha)} & 0 \\ 0 & \boldsymbol{\Lambda}_k^{(\alpha)} \end{bmatrix}, \quad \tilde{F}^{(\alpha)} = \tilde{\boldsymbol{\Phi}}^{(\alpha)\mathrm{T}} \hat{\boldsymbol{F}}^{(\alpha)}, \end{aligned}\right\} \tag{4.30}$$

where $\boldsymbol{T}^{(\alpha)}$ represents the transformation matrix from a global degree of freedom $\bar{\boldsymbol{Q}}$ of the structure to a degree of freedom $\tilde{\boldsymbol{Q}}^{(\alpha)}$ of the α substructure. For example, if $\mathrm{Sub_s} = 2$, the global degree of freedom of the structure can be represented as

$$\bar{\boldsymbol{Q}} = \begin{bmatrix} Q_k^{(1)} \\ U^j \\ Q_k^{(2)} \end{bmatrix}. \tag{4.31}$$

It is noted that the synthesis computations defined in equations (4.30) can be implemented in a similar way to the assembly of finite-element matrices. As required by the functional H_{s} in equation (3.5), the only necessary condition for synthesis is the consistency of displacement between adjacent interfaces of substructures.

It is not difficult to realize that the finite-element solution of the original problem can be obtained by this mode synthesis method without any mode reduction, relying on the independence between the consistent displacement modes and the normalized modes of substructures with fixed interfaces. In fact, the finite-element equation of the original structure can be easily obtained through an inverse-transformation of equation (4.27). In the mode reduction case, the solution produced by mode synthesis is inherently a good approximation to the solution of the original problem because mode reduction is carried out according to the magnitude of the mode factors relevant to the substructure.

5. Hybrid displacement model of solid substructure

By means of the application of the Lagrange multiplier method, the consistent condition of the displacement or acceleration between the interface of two adjacent substructures can be released from the functional in equation (3.5). A modified func-

tional in the form

$$H_{Is}[\ddot{\boldsymbol{U}}, F^j] = \sum_{\alpha=1}^{\mathrm{Sub_s}} \int_{t_1}^{t_2} (\tfrac{1}{2}\ddot{\boldsymbol{U}}^{\mathrm{T}}\boldsymbol{M}\ddot{\boldsymbol{U}} - \tfrac{1}{2}\dot{\boldsymbol{U}}^{\mathrm{T}}\boldsymbol{K}\dot{\boldsymbol{U}} - \ddot{\boldsymbol{U}}^{\mathrm{T}}\hat{\boldsymbol{F}} - \ddot{U}^{j\mathrm{T}}F^j)^{(\alpha)}\,\mathrm{d}t, \tag{5.1}$$

can be obtained. Here, F^j denotes the Lagrange multiplier, and physically it represents the forces on the interface of two adjacent substructures. This functional requires that the equilibrium condition of the forces on the interface of two adjacent substructures, for example, the condition in equation (4.3) for case $\mathrm{Sub_s} = 2$ must be satisfied. When using this functional to formulate the substructure model, the chosen collection of mode vectors must guarantee the equilibrium of interface forces between two adjacent substructures. On the other hand, the consistent condition of displacement or acceleration, which is not pre-imposed, can be obtained through the variation of the functional in equation (5.1). In fact, for the case of $\mathrm{Sub_s} = 2$ it follows that by using the consistent force condition expressed in equation (4.3), the dynamical equations describing the substructures in equation (4.2) and the consistent acceleration condition on the interface of two adjacent substructures, i.e.

$$\ddot{U}^{j(1)} = \ddot{U}^{j(2)}, \tag{5.2}$$

are derived from the variation of the functional in equation (5.1). It is on such a theoretical base that a hybrid displacement model of solid substructure can be established.

(*a*) *Sets of mode vector*

For the hybrid displacement model, two requirements must be satisfied in the selection of the collection of mode vectors. They are (*a*) the condition of consistent force between the interfaces of two adjacent substructures, and (*b*) a full description of the motion configurations of the substructure in space. To develop this model, let us take

$$\boldsymbol{U} = \boldsymbol{U}_1 + \boldsymbol{U}_0, \tag{5.3}$$

$$\boldsymbol{K}\boldsymbol{U}_0 = \begin{bmatrix} 0 \\ F^j \end{bmatrix}, \tag{5.4}$$

$$\boldsymbol{M}\ddot{\boldsymbol{U}}_1 + \boldsymbol{K}\boldsymbol{U}_1 = -\boldsymbol{M}\ddot{\boldsymbol{U}}_0 + \hat{\boldsymbol{F}}. \tag{5.5}$$

We can now define the following two kinds of modes.

(i) *Consistent force modes between interfaces* These modes are defined by the static configuration of the substructure when a unit force is applied successively to each degree of freedom on its interfaces, with all remaining freedom-degrees unfettered. This collection of consistent force mode vectors is given by

$$\boldsymbol{y} = \boldsymbol{K}^{-1}\begin{bmatrix} 0 \\ I^{jj} \end{bmatrix} = \boldsymbol{\Phi}_{\mathrm{e}}\boldsymbol{\Lambda}_{\mathrm{e}}^{-1}\boldsymbol{\Phi}_{\mathrm{e}}^{j\mathrm{T}}, \tag{5.6}$$

$$\boldsymbol{U}_0 = \boldsymbol{y}F^j, \tag{5.7}$$

where the subscript 'e' indicates that the elastic modes of the substructure are referred to in the associated quantities. Furthermore, we assume that the matrix $\boldsymbol{K}$ has an inverse. If it is not so, a frequency shift technique can be applied as discussed in § 8 *a*.

(ii) *Normalized modes for free interface substructure* These are the normalized vibration shapes associated with the interface of the substructure when allowed complete freedom from all constraints. In terms of generalized coordinates, equation (5.5) with $\hat{\boldsymbol{F}} = 0$, can be rewritten as

$$\boldsymbol{U}_1 = \boldsymbol{\Phi}_{\mathrm{e}} Q_{\mathrm{e}}, \qquad \boldsymbol{\Phi}_{\mathrm{e}}^{\mathrm{T}} \boldsymbol{M} \boldsymbol{\Phi}_{\mathrm{e}} = \boldsymbol{I}, \qquad \boldsymbol{\Phi}_{\mathrm{e}}^{\mathrm{T}} \boldsymbol{K} \boldsymbol{\Phi}_{\mathrm{e}} = \boldsymbol{\Lambda}_{\mathrm{e}}, \tag{5.8}$$

$$\begin{aligned} Q_{\mathrm{e}} &= \Omega^2 (\boldsymbol{\Lambda}_{\mathrm{e}} - \Omega^2 \boldsymbol{I})^{-1} \boldsymbol{\Phi}_{\mathrm{e}}^{\mathrm{T}} \boldsymbol{M} \boldsymbol{K}^{-1} \begin{bmatrix} 0 \\ F^j \end{bmatrix} \\ &= \Omega^2 (\boldsymbol{\Lambda}_{\mathrm{e}} - \Omega^2 \boldsymbol{I})^{-1} \boldsymbol{\Lambda}_{\mathrm{e}}^{-1} \boldsymbol{\Phi}_{\mathrm{e}}^{\mathrm{T}} \begin{bmatrix} 0 \\ F^j \end{bmatrix}, \end{aligned} \tag{5.9}$$

allowing the following factors to be defined.

The mode factor

$$q_s = \frac{\Omega^2}{\omega_s^2 (\omega_s^2 - \Omega^2)} \phi_s^{\mathrm{T}} \begin{bmatrix} 0 \\ F^j \end{bmatrix} = \frac{\Omega^2}{\omega_s^2 (\omega_s^2 - \Omega^2)} \phi_s^{j\mathrm{T}} F^j. \tag{5.10}$$

The frequency factor

$$q_{s\omega} = \frac{\Omega^2}{\omega_s^2 - \Omega^2} \approx \begin{cases} -1 & \text{if } \omega_s \ll \Omega, \\ \Omega^2/\omega_s^2 & \text{if } \omega_s \gg \Omega. \end{cases} \tag{5.11}$$

The vibration shape factor

$$q_{s\phi} = \phi_s^{\mathrm{T}} M K^{-1} \begin{bmatrix} 0 \\ F^j \end{bmatrix} = \frac{1}{\omega_s^2} \phi_s^{j\mathrm{T}} F^j. \tag{5.12}$$

The motion of the substructure can now be described by the equation

$$\boldsymbol{U} = \boldsymbol{y} F^j + \boldsymbol{\Phi}_{\mathrm{e}} Q_{\mathrm{e}}, \tag{5.13}$$

where $\boldsymbol{y}$ and $\boldsymbol{\Phi}$ are the collections of mode vectors corresponding to the generalized coordinates F^j and Q_{e}, respectively. Evidently, $\boldsymbol{y}$ and $\boldsymbol{\Phi}$ are not independent of one another, but they can be arranged to be so after mode reduction.

(*b*) *Rule and method of mode reduction*

The rule applied to mode reduction in this hybrid model is that under a consistent force condition between the interface of substructures, we retain the substructural modes which provide significant contribution to the modes of the structure and neglect those producing little contribution to the global structure modes. Therefore, the number of elastic modes associated with the free interface substructure may be reduced. The reduction method applicable to this situation is similar to the one used in the consistent displacement model. To guarantee the independence of various mode vectors, after reduction the consistent modes are corrected by the relation,

$$\boldsymbol{\xi} = \boldsymbol{y} - \boldsymbol{\Phi}_k \boldsymbol{\Lambda}_k^{-1} \Phi_k^{j\mathrm{T}} = \boldsymbol{\Phi}_h \boldsymbol{\Lambda}_h^{-1} \Phi_h^{j\mathrm{T}}, \tag{5.14}$$

allowing the corresponding motion of the substructure to be rewritten in the form,

$$\boldsymbol{U} = \boldsymbol{\xi} \mu^j + \boldsymbol{\Phi}_k Q_k. \tag{5.15}$$

Here the subscripts k and h denote the retained modes and the higher modes which have been reduced, respectively. Thus μ^j is the generalized coordinate corresponding

to the mode vector $\boldsymbol{\xi}$ satisfying the equilibrium condition. For example, for $\mathrm{Sub_s} = 2$

$$\mu^{j(1)} + \mu^{j(2)} = 0, \tag{5.16}$$

and the collection of mode vectors $\boldsymbol{\xi}$ and $\boldsymbol{\Phi}_k$ satisfy the orthogonal relations,

$$\boldsymbol{\xi}^{\mathrm{T}}\boldsymbol{M}\boldsymbol{\Phi}_k = 0, \qquad \boldsymbol{\xi}^{\mathrm{T}}\boldsymbol{K}\boldsymbol{\Phi}_k = 0. \tag{5.17}$$

These results can be confirmed by using equations (5.8) and (5.14).

From equations (5.6), (5.9) and (5.13), the component of the displacement U^j satisfies the equation

$$U^j = \{\Phi_{\mathrm{e}}^j \boldsymbol{\Lambda}_{\mathrm{e}}^{-1} \Phi_{\mathrm{e}}^{j\mathrm{T}} + \Phi_{\mathrm{e}}^j \Omega^2 (\boldsymbol{\Lambda}_{\mathrm{e}} - \Omega^2 \boldsymbol{I})^{-1} \boldsymbol{\Lambda}_{\mathrm{e}}^{-1} \Phi_{\mathrm{e}}^{j\mathrm{T}}\} F^j = G^{jj} F^j, \tag{5.18}$$

where G^{jj} is referred to as the dynamical compliance of the substructure interface. The factor $(\boldsymbol{\Lambda}_{\mathrm{e}} - \Omega^2 \boldsymbol{I})^{-1}$ is positive definite if $\omega_s^2 > \Omega^2$ and negative definite if $\omega_s^2 < \Omega^2$. Therefore, the neglect of a mode with frequency higher than Ω of the substructure reduces the value of the dynamical compliance, implying that the interface of substructure is harder; the reverse case makes the interface of substructure softer (i.e. more flexible). These results are similar to the ones obtained in the consistent displacement model, and therefore the previous conclusion relating to the effect of frequency reduction is valid. Obviously, if no modes are reduced, then $\boldsymbol{\xi} = \boldsymbol{0}$, and the solution obtained by this mode synthesis method is replaced by the solution obtained from the corresponding finite-element method.

(*c*) *Synthesis of substructure equations*

Calculations through synthesis can be derived by using equations (5.1), (5.2) and (5.15). The mode transformation relation in equation (5.15) for substructure (α) can be rewritten as

$$\boldsymbol{U}^{(\alpha)} = [\boldsymbol{\xi}^{(\alpha)} \quad \boldsymbol{\Phi}_k^{(\alpha)}] \begin{bmatrix} \mu^{j(\alpha)} \\ Q_k^{(\alpha)} \end{bmatrix} = \tilde{\boldsymbol{\Phi}}^{(\alpha)} \tilde{\boldsymbol{Q}}^{(\alpha)}. \tag{5.19}$$

The respective displacement and acceleration on the interface of a substructure are given by

$$U^{j(\alpha)} = [\boldsymbol{\xi}^{j(\alpha)} \quad \Phi_k^{j(\alpha)}] \begin{bmatrix} \mu^{j(\alpha)} \\ Q_k^{(\alpha)} \end{bmatrix} = \tilde{\Phi}^{j(\alpha)} \tilde{\boldsymbol{Q}}^{(\alpha)}, \tag{5.20}$$

and

$$\ddot{U}^{j(\alpha)} = [\boldsymbol{\xi}^{j(\alpha)} \quad \Phi_k^{j(\alpha)}] \begin{bmatrix} \ddot{\mu}^{j(\alpha)} \\ \ddot{Q}_k^{(\alpha)} \end{bmatrix} = \tilde{\Phi}^{j(\alpha)} \ddot{\tilde{\boldsymbol{Q}}}^{(\alpha)}. \tag{5.21}$$

The substitution of equation (5.19) into equation (5.1) gives

$$H_{Is} = \sum_{\alpha=1}^{\mathrm{Sub_s}} \int_{t_1}^{t_2} (\tfrac{1}{2} \ddot{\tilde{\boldsymbol{Q}}}^{\mathrm{T}} \tilde{\boldsymbol{M}} \ddot{\tilde{\boldsymbol{Q}}} - \tfrac{1}{2} \dot{\tilde{\boldsymbol{Q}}}^{\mathrm{T}} \tilde{\boldsymbol{K}} \dot{\tilde{\boldsymbol{Q}}} - \ddot{\tilde{\boldsymbol{Q}}}^{\mathrm{T}} \tilde{\boldsymbol{F}} - \ddot{\tilde{\boldsymbol{Q}}}^{\mathrm{T}} \tilde{F}^j)^{(\alpha)} \, \mathrm{d}t, \tag{5.22}$$

and by means of the variation of equation (5.22) in conjunction with equations (5.8) and (5.17), we derive the following equations:

$$\bar{\boldsymbol{M}} \ddot{\bar{\boldsymbol{Q}}} + \bar{\boldsymbol{K}} \bar{\boldsymbol{Q}} = \bar{\boldsymbol{F}} + \bar{\boldsymbol{F}}^j, \tag{5.23}$$

and

$$\bar{\boldsymbol{Q}}^{\mathrm{T}} \sum_{\alpha=1}^{\mathrm{Sub_s}} \boldsymbol{T}^{(\alpha)\mathrm{T}} \tilde{\boldsymbol{\phi}}^{j(\alpha)\mathrm{T}} \tilde{\boldsymbol{T}}^{(\alpha)} = 0. \tag{5.24}$$

The quantities occurring in equations (5.20)–(5.24) are defined by

$$\left.\begin{gathered} \tilde{\boldsymbol{Q}}^{(\alpha)} = \boldsymbol{T}^{(\alpha)} \bar{\boldsymbol{Q}}, \quad \bar{M} = \sum_{\alpha=1}^{\mathrm{Sub_s}} \boldsymbol{T}^{(\alpha)\mathrm{T}} \tilde{\boldsymbol{M}}^{(\alpha)} \boldsymbol{T}^{(\alpha)}, \\ \bar{\boldsymbol{K}} = \textstyle\sum_{\alpha=1}^{\mathrm{Sub_s}} \boldsymbol{T}^{(\alpha)\mathrm{T}} \tilde{\boldsymbol{K}}^{(\alpha)} \boldsymbol{T}^{(\alpha)}, \quad \bar{\boldsymbol{F}} = \textstyle\sum_{\alpha=1}^{\mathrm{Sub_s}} \boldsymbol{T}^{(\alpha)\mathrm{T}} \tilde{\boldsymbol{F}}^{(\alpha)}, \quad \boldsymbol{F}^{j} = \textstyle\sum_{\alpha=1}^{\mathrm{Sub_s}} \boldsymbol{T}^{(\alpha)\mathrm{T}} \tilde{F}^{j(\alpha)}, \\ \tilde{\boldsymbol{M}}^{(\alpha)} = \begin{bmatrix} \boldsymbol{\xi}^{(\alpha)\mathrm{T}} \boldsymbol{M}^{(\alpha)} \boldsymbol{\xi}^{(\alpha)} & 0 \\ 0 & I_k^{(\alpha)} \end{bmatrix}, \quad \tilde{\boldsymbol{K}}^{(\alpha)} = \begin{bmatrix} \boldsymbol{\xi}^{(\alpha)\mathrm{T}} \boldsymbol{K}^{(\alpha)} \boldsymbol{\xi}^{(\alpha)} & 0 \\ 0 & \Lambda_k^{(\alpha)} \end{bmatrix}, \\ \tilde{\boldsymbol{F}}^{(\alpha)} = \tilde{\boldsymbol{\phi}}^{(\alpha)\mathrm{T}} \hat{\boldsymbol{F}}^{(\alpha)}, \quad \tilde{F}^{j(\alpha)} = \tilde{\boldsymbol{\phi}}^{j(\alpha)\mathrm{T}} F^{j(\alpha)}, \quad F^{j(\alpha)} = \tilde{\boldsymbol{T}}^{(\alpha)} \bar{F}^{j}, \end{gathered}\right\} \tag{5.25}$$

where $\boldsymbol{T}^{(\alpha)}$ represents the transformation matrix from the global degree of freedom $\bar{\boldsymbol{Q}}$ of the structure to the degree of freedom $\tilde{\boldsymbol{Q}}^{(\alpha)}$ of the α substructure, and $\tilde{\boldsymbol{T}}^{(\alpha)}$ represents the transformation matrix from the independent interface force vector $\bar{F}^{j}$ to the interface force vector $F^{j(\alpha)}$ of the α substructure. For example, in the case of $\mathrm{Sub_s} = 2$ illustrated in figure 2, these quantities have the following forms:

$$\bar{\boldsymbol{Q}} = \begin{bmatrix} Q_k^{(1)} \\ \mu^{j} \\ Q_k^{(2)} \end{bmatrix}, \tag{5.26}$$

and

$$\bar{F}^{j} = F^{j(1)}. \tag{5.27}$$

We find that by using equation (5.24), the dependent variable can be reduced, so that

$$\bar{\boldsymbol{Q}} = \breve{\boldsymbol{T}} \breve{\boldsymbol{Q}}, \tag{5.28}$$

allowing the transformation of equation (5.23) to its final form

$$\breve{\boldsymbol{M}} \ddot{\breve{\boldsymbol{Q}}} + \breve{\boldsymbol{K}} \breve{\boldsymbol{Q}} = \breve{\boldsymbol{F}}. \tag{5.29}$$

Here,

$$\breve{\boldsymbol{M}} = \breve{\boldsymbol{T}}^{\mathrm{T}} \bar{\boldsymbol{M}} \breve{\boldsymbol{T}}, \qquad \breve{\boldsymbol{K}} = \breve{\boldsymbol{T}}^{\mathrm{T}} \bar{\boldsymbol{K}} \breve{\boldsymbol{T}}, \qquad \breve{\boldsymbol{F}} = \breve{\boldsymbol{T}}^{\mathrm{T}} \bar{\boldsymbol{F}}, \tag{5.30}$$

from which it can be deduced that

$$\breve{\boldsymbol{T}}^{\mathrm{T}} \bar{\boldsymbol{F}}^{j} = 0. \tag{5.31}$$

This process can be implemented in the same way as adopted to assemble finite-element matrices.

6. Pressure equilibrium model of fluid subdomain

In a similar way to the development of a consistent displacement model for a solid substructure, a pressure equilibrium model for a fluid subdomain can be constructed

based on the functional in equation (3.6). In this model, the pressure equilibrium condition on the interface between two adjacent subdomains must be satisfied. Therefore, the mode vectors must be suitably chosen (i) to guarantee the pressure equilibrium on interfaces and (ii) to construct a complete subspace. These are similar to the conditions imposed in the displacement consistency model in § 4.

Taking the variation of the functional (3.6), we obtain

$$\delta H_{\mathrm{f}}[p] = \sum_{\beta=1}^{\mathrm{Sub_f}} \int_{t_1}^{t_2} (\delta \dot{\boldsymbol{p}}^{\mathrm{T}} \boldsymbol{m} \dot{\boldsymbol{p}} - \delta \boldsymbol{p}^{\mathrm{T}} \boldsymbol{k} \boldsymbol{p} - \delta \boldsymbol{p}^{\mathrm{T}} \hat{\ddot{\boldsymbol{u}}})^{(\beta)} \, \mathrm{d}t$$

$$= \sum_{\beta=1}^{\mathrm{Sub_f}} \int_{t_1}^{t_2} \delta \boldsymbol{p}^{\mathrm{T}} (-\boldsymbol{m} \ddot{\boldsymbol{p}} - \boldsymbol{k} \boldsymbol{p} - \hat{\ddot{\boldsymbol{u}}})^{(\beta)} \, \mathrm{d}t. \tag{6.1}$$

Because of the independence of $\delta \boldsymbol{p}$ and by using the variation $\delta H_{\mathrm{f}} = 0$, we derive an equation describing the dynamical behaviour of the pressure fluid element which, in subdomain form, can be expressed as

$$\begin{bmatrix} m^{ii} & m^{ij} \\ m^{ji} & m^{jj} \end{bmatrix}^{(\beta)} \begin{bmatrix} \ddot{p}^i \\ \ddot{p}^j \end{bmatrix}^{(\beta)} + \begin{bmatrix} k^{ii} & k^{ij} \\ k^{ji} & k^{jj} \end{bmatrix}^{(\beta)} \begin{bmatrix} p^i \\ p^j \end{bmatrix}^{(\beta)} = \begin{bmatrix} -\hat{\ddot{u}}^i \\ -\hat{\ddot{u}}^j \end{bmatrix}^{(\beta)} + \begin{bmatrix} 0 \\ -\ddot{u}^j \end{bmatrix}^{(\beta)}, \tag{6.2}$$

$$\sum_{\beta=1}^{\mathrm{Sub_f}} -\ddot{u}^{j(\beta)} = 0. \tag{6.3}$$

Here superscript i represents the number of internal degrees of freedom assumed in the subdomain, the superscript j represents the number of degrees of freedom on the interface of two adjacent subdomains and the quantity $-\ddot{u}^j$ denotes the interface acceleration on the interface of the subdomain. No summation convention is applied to superscripts i and j.

From a mathematical point of view, equations (6.1), (6.2) and (6.3) are similar to equations (4.1), (4.2) and (4.3) for the consistent displacement model for a solid substructure. For this reason, no discussion is presented of the process to derive the pressure equilibrium model for the fluid subdomain. Here we focus on the procedure to derive the set of modes for this model and their corresponding synthesis.

(*a*) *Sets of mode vector*

(i) *Pressure equilibrium modes between interfaces*

These relate to the pressure distribution within the subdomain with the fluid compressibility neglected. (This is comparable to the approach adopted in deriving equation (4.5) in which the inertia forces are neglected.) That is, the velocity of sound in the fluid $c \to \infty$, and a unit pressure is imposed successively to each degree of freedom along the interface with all the other degrees of freedom along the interface set to zero pressure. By virtue of matrix notation and by repeating a similar analysis to the one discussed in § 4, we derive the expression

$$\begin{bmatrix} k^{ii} & k^{ij} \\ k^{ji} & k^{jj} \end{bmatrix} \begin{bmatrix} Y^{ij} \\ I^{jj} \end{bmatrix} = \begin{bmatrix} 0 \\ -\ddot{u}_0^{jj} \end{bmatrix}. \tag{6.4}$$

This result allows the collection of pressure equilibrium modes between interfaces to be defined as

$$\boldsymbol{Y} = \begin{bmatrix} Y^{ij} \\ I^{jj} \end{bmatrix} = \begin{bmatrix} -(k^{ii})^{-1}k^{ij} \\ I^{jj} \end{bmatrix}, \tag{6.5}$$

where I^{jj} is a unit matrix.

(ii) *Normalized pressure modes of a zero pressure interface subdomain*

These are the normalized natural vibration pressure mode shapes associated with the interfaces of the subdomain kept at zero pressure. They are calculated by solving the following eigenvalue equation:

$$m^{ii}\ddot{p}_1^i + k^{ii}p_1^i = 0, \tag{6.6}$$

$$p_1^i = \varphi^i P, \qquad \varphi^{i\mathrm{T}} m^{ii} \varphi^i = I^{ii}, \qquad \varphi^{i\mathrm{T}} k^{ii} \varphi^i = \lambda, \tag{6.7}$$

where φ^i is the matrix of normalized pressure modes, P denotes the generalized coordinate vector and the diagonal matrix $\lambda = \mathrm{diag}(\omega_s^2)$ relates to the the square of a natural frequency ω_s of the subdomain.

By combining these collections of mode vectors (i.e. $\boldsymbol{Y}$ and $\boldsymbol{\varphi}$), we find that the pressure in the subdomain can be written in the form

$$\boldsymbol{p} = \boldsymbol{Y}p^j + \boldsymbol{\varphi}P, \tag{6.8}$$

where the base vectors of the subdomain pressure space are the pressure equilibrium modes $\boldsymbol{Y}$ in equation (6.5) and the normalized pressure modes of the subdomain with zero pressure interface, i.e.

$$\boldsymbol{\varphi} = \begin{bmatrix} \varphi^i \\ 0 \end{bmatrix}. \tag{6.9}$$

The corresponding generalized coordinate vectors are the interface pressure p^j for the base vector $\boldsymbol{Y}$ and the generalized coordinate P for the normalized pressure mode vectors.

(*b*) *Synthesis of subdomain equations*

Let $\boldsymbol{\varphi}_k^{(\beta)}$ and $\boldsymbol{P}_k^{(\beta)}$ denote the retained normalized modes of subdomain (β) and the corresponding generalized coordinate respectively. It follows from equation (6.8) that the pressure in this subdomain (β) can be written as

$$\boldsymbol{p}^{(\beta)} = [\boldsymbol{Y}^{(\beta)} \quad \boldsymbol{\varphi}_k^{(\beta)}] \begin{bmatrix} p^{j(\beta)} \\ P_k^{(\beta)} \end{bmatrix}, \tag{6.10}$$

or simply,

$$\boldsymbol{p}^{(\beta)} = \tilde{\boldsymbol{\varphi}}^{(\beta)} \tilde{\boldsymbol{P}}^{(\beta)}. \tag{6.11}$$

The substitution of equation (6.11) into equation (3.6) gives

$$H_{\mathrm{f}} = \sum_{\beta=1}^{\mathrm{Sub_f}} \int_{t_1}^{t_2} (\tfrac{1}{2}\dot{\tilde{\boldsymbol{P}}}^{\mathrm{T}} \tilde{\boldsymbol{m}} \dot{\tilde{\boldsymbol{P}}} - \tfrac{1}{2}\tilde{\boldsymbol{P}}^{\mathrm{T}} \tilde{\boldsymbol{k}} \tilde{\boldsymbol{P}} - \tilde{\boldsymbol{P}}^{\mathrm{T}} \ddot{\tilde{\boldsymbol{u}}})^{(\beta)} \, \mathrm{d}t, \tag{6.12}$$

and by means of the variation of equation (6.12), the dynamical equation after synthesis satisfies the relationship,

$$\bar{\boldsymbol{m}}\ddot{\bar{\boldsymbol{P}}} + \bar{\boldsymbol{k}}\bar{\boldsymbol{P}} = \bar{\boldsymbol{f}}. \tag{6.13}$$

The quantities occurring in these equations are given by

$$\left.\begin{aligned} \tilde{\boldsymbol{P}}^{(\beta)} &= \boldsymbol{T}^{(\beta)}\bar{\boldsymbol{P}}, \quad \bar{\boldsymbol{m}} = \sum_{\beta=1}^{\mathrm{Sub_f}} \boldsymbol{T}^{(\beta)\mathrm{T}}\tilde{\boldsymbol{m}}^{(\beta)}\boldsymbol{T}^{(\beta)}, \\ \bar{\boldsymbol{k}} &= \sum_{\beta=1}^{\mathrm{Sub_f}} \boldsymbol{T}^{(\beta)\mathrm{T}}\tilde{\boldsymbol{k}}^{(\beta)}\boldsymbol{T}^{(\beta)}, \quad \bar{\boldsymbol{f}} = \sum_{\beta=1}^{\mathrm{Sub_f}} -\boldsymbol{T}^{(\beta)\mathrm{T}}\ddot{\tilde{\boldsymbol{u}}}^{(\beta)}, \\ \tilde{\boldsymbol{m}}^{(\beta)} &= \begin{bmatrix} \boldsymbol{Y}^{(\beta)\mathrm{T}}\boldsymbol{m}^{(\beta)}\boldsymbol{Y}^{(\beta)} & \boldsymbol{Y}^{(\beta)\mathrm{T}}\boldsymbol{m}^{(\beta)}\boldsymbol{\varphi}_k^{(\beta)} \\ \boldsymbol{\varphi}_k^{(\beta)\mathrm{T}}\boldsymbol{m}^{(\beta)}\boldsymbol{Y}^{(\beta)} & \boldsymbol{I}_k^{(\beta)} \end{bmatrix}, \\ \tilde{\boldsymbol{k}}^{(\beta)} &= \begin{bmatrix} \boldsymbol{Y}^{(\beta)\mathrm{T}}\boldsymbol{k}^{(\beta)}\boldsymbol{Y}^{(\beta)} & 0 \\ 0 & \boldsymbol{\lambda}_k^{(\beta)} \end{bmatrix}, \\ \ddot{\tilde{\boldsymbol{u}}}^{(\beta)} &= \tilde{\boldsymbol{\varphi}}^{(\beta)\mathrm{T}}\ddot{\hat{\boldsymbol{u}}}^{(\beta)}. \end{aligned}\right\} \tag{6.14}$$

Here $\boldsymbol{T}^{(\beta)}$ represents the transformation matrix from the global degree of freedom $\bar{\boldsymbol{P}}$ of the fluid domain to the degree of freedom $\tilde{\boldsymbol{P}}^{(\beta)}$ of the β-subdomain.

This synthesis process can be implemented in the same way as usually adopted when assembling finite-element matrices. As required by the functional H_{f} in equation (3.6), the pressure equilibrium condition on the interfaces of two adjacent subdomains is the only necessary requirement to be satisfied for synthesis to take place.

7. Mixed model of substructure–subdomain

For a coupled fluid–solid interaction problem, the functional (3.4) can be used to construct a model connecting a substructure and a subdomain. For simplicity, let us discuss the case of $\mathrm{Sub^s} = 1$ and $\mathrm{Sub^f} = 1$. The variation of the functional (3.4) now takes the form:

$$\begin{aligned} \delta H_{\mathrm{sf}} &= \int_{t_1}^{t_2} (\delta\ddot{\boldsymbol{U}}^{\mathrm{T}}\boldsymbol{M}\ddot{\boldsymbol{U}} - \delta\dot{\boldsymbol{U}}^{\mathrm{T}}\boldsymbol{K}\dot{\boldsymbol{U}} - \delta\ddot{\boldsymbol{U}}^{\mathrm{T}}\hat{\boldsymbol{F}})\,\mathrm{d}t \\ &\quad + \int_{t_1}^{t_2} (\delta\dot{\boldsymbol{p}}^{\mathrm{T}}\boldsymbol{m}\dot{\boldsymbol{p}} - \delta\boldsymbol{p}^{\mathrm{T}}\boldsymbol{k}\boldsymbol{p} - \delta\boldsymbol{p}^{\mathrm{T}}\ddot{\hat{\boldsymbol{u}}})\,\mathrm{d}t - \int_{t_1}^{t_2} (\delta\boldsymbol{p}^{\mathrm{T}}\boldsymbol{R}\ddot{\boldsymbol{U}} + \delta\ddot{\boldsymbol{U}}^{\mathrm{T}}\boldsymbol{R}^{\mathrm{T}}\boldsymbol{p})\,\mathrm{d}t \\ &= \int_{t_1}^{t_2} \{\delta\ddot{\boldsymbol{U}}^{\mathrm{T}}(\boldsymbol{M}\ddot{\boldsymbol{U}} + \boldsymbol{K}\boldsymbol{U} - \hat{\boldsymbol{F}} - \boldsymbol{R}^{\mathrm{T}}\boldsymbol{p})\,\mathrm{d}t - \delta\boldsymbol{p}^{\mathrm{T}}(\boldsymbol{m}\ddot{\boldsymbol{p}} + \boldsymbol{k}\boldsymbol{p} + \ddot{\hat{\boldsymbol{u}}} + \boldsymbol{R}\ddot{\boldsymbol{U}})\}\,\mathrm{d}t. \end{aligned} \tag{7.1}$$

Because of the independence of the variations $\delta\ddot{U}$ and $\delta\boldsymbol{p}$, the equations describing dynamical interaction between an adjacent substructure–subdomain are

$$\begin{bmatrix} M^{ii} & M^{ic} \\ M^{ci} & M^{cc} \end{bmatrix} \begin{bmatrix} \ddot{U}^i \\ \ddot{U}^c \end{bmatrix} + \begin{bmatrix} K^{ii} & K^{ic} \\ K^{ci} & K^{cc} \end{bmatrix} \begin{bmatrix} U^i \\ U^c \end{bmatrix} = \bar{\boldsymbol{R}}^{\mathrm{T}} \begin{bmatrix} p^i \\ p^c \end{bmatrix} + \begin{bmatrix} \hat{F}^i \\ \hat{F}^c \end{bmatrix} \tag{7.2}$$

for a solid substructure, and

$$\begin{bmatrix} m^{ii} & m^{ic} \\ m^{ci} & m^{cc} \end{bmatrix} \begin{bmatrix} \ddot{p}^i \\ \ddot{p}^c \end{bmatrix} + \begin{bmatrix} k^{ii} & k^{ic} \\ k^{ci} & k^{cc} \end{bmatrix} \begin{bmatrix} p^i \\ p^c \end{bmatrix} = -\bar{\boldsymbol{R}} \begin{bmatrix} \ddot{U}^i \\ \ddot{U}^c \end{bmatrix} + \begin{bmatrix} \hat{f}^i \\ \hat{f}^c \end{bmatrix} \tag{7.3}$$

for a fluid domain. Here, we have

$$\bar{\boldsymbol{R}} = \begin{bmatrix} 0 & 0 \\ 0 & \boldsymbol{R} \end{bmatrix}, \qquad \hat{f}^i = -\hat{\ddot{u}}^i, \qquad \hat{f}^c = -\hat{\ddot{u}}^c, \tag{7.4}$$

and the superscript c represents the number of degrees of freedom on the coupling fluid–solid interface between the substructure and subdomain.

The functional in equation (3.4) does not require any prerequisite form of consistency of displacement or acceleration and pressure on the coupled interface between fluid and solid, so there can exist many collections of mode vectors associated with the mixed substructure–subdomain model (see Xing 1984, 1986*a*, *b*). Here, one collection of mode vectors is described. This represents a model of pressure equilibrium on a coupled interface.

(*a*) *Set of mode vectors*

To advance our argument, firstly let us assume that the pressure on the interface between the fluid and solid is zero. Physically this implies no fluid–solid interaction. In this situation, the fluid subdomain and the solid substructure can be solved separately and an initial selection of their respective mode vectors obtained. Then we consider the practical case of a pressure acting on the coupled interface to correct for the first selection of mode vectors.

Mathematically, as in the previous §§ 4–6 the displacement U and pressure p can be divided into two parts

$$\boldsymbol{U} = \boldsymbol{U}_1 + \boldsymbol{U}_0, \tag{7.5}$$

$$\begin{bmatrix} p^i \\ p^c \end{bmatrix} = \begin{bmatrix} p_1^i \\ 0 \end{bmatrix} + \begin{bmatrix} p_0^i \\ p^c \end{bmatrix}, \tag{7.6}$$

where each part of the displacement and pressure satisfies the equations

$$\boldsymbol{K}\boldsymbol{U}_0 = \begin{bmatrix} 0 \\ \boldsymbol{R}^{\mathrm{T}} p^c \end{bmatrix}, \tag{7.7}$$

$$\boldsymbol{M}\ddot{\boldsymbol{U}}_1 + \boldsymbol{K}\boldsymbol{U}_1 = -\boldsymbol{M}\ddot{\boldsymbol{U}}_0 + \hat{\boldsymbol{F}}, \tag{7.8}$$

and

$$\begin{bmatrix} k^{ii} & k^{ic} \\ k^{ci} & k^{cc} \end{bmatrix} \begin{bmatrix} p_0^i \\ p^c \end{bmatrix} = \begin{bmatrix} 0 \\ -\boldsymbol{R}\ddot{U}_0^c \end{bmatrix}, \tag{7.9}$$

$$\begin{bmatrix} m^{ii} & m^{ic} \\ m^{ci} & m^{cc} \end{bmatrix} \begin{bmatrix} \ddot{p}_1^i \\ 0 \end{bmatrix} + \begin{bmatrix} k^{ii} & k^{ic} \\ k^{ci} & k^{cc} \end{bmatrix} \begin{bmatrix} p_1^i \\ 0 \end{bmatrix} = \begin{bmatrix} \hat{f}^i \\ \hat{f}^c \end{bmatrix} - \begin{bmatrix} 0 \\ \boldsymbol{R}\ddot{U}_1^c \end{bmatrix} - \begin{bmatrix} m^{ii} & m^{ic} \\ m^{ci} & m^{cc} \end{bmatrix} \begin{bmatrix} \ddot{p}_0^i \\ \ddot{p}^c \end{bmatrix}. \tag{7.10}$$

Comparing equations (7.5), (7.7) and (7.8) with equations (5.3), (5.4) and (5.5), we find that the set of mode vectors for the hybrid displacement model of solid substructure can be used to represent the motion of this substructure with fluid–solid interaction interface. That is

$$\boldsymbol{U} = [\boldsymbol{\xi} \quad \boldsymbol{\Phi}_k] \begin{bmatrix} \mu^c \\ Q_k \end{bmatrix} = \tilde{\boldsymbol{\Phi}}\tilde{\boldsymbol{Q}}. \tag{7.11}$$

Similarly, from a comparison of equations (7.6), (7.9) and (7.10) with the equations related to the pressure equilibrium model for a fluid subdomain in §6, the fluid pressure in the fluid subdomain with the fluid–solid interaction interface can be represented as

$$\boldsymbol{p} = [\boldsymbol{Y} \quad \boldsymbol{\varphi}_k] \begin{bmatrix} p^c \\ P_k \end{bmatrix} = \tilde{\boldsymbol{\varphi}}\tilde{\boldsymbol{P}}. \tag{7.12}$$

In this model, the mode vectors $\boldsymbol{\xi}$, $\boldsymbol{\Phi}_k$, $\boldsymbol{Y}$ and $\boldsymbol{\varphi}_k$ are respectively given in equations (5.14), (5.8), (6.5) and (6.7) with the superscript c replacing j.

The mode reduction process is similar to the one previously discussed in §§4*c*, 5*c* and 6*b* and no additional explanation is needed.

(*b*) *Synthesis of substructure–subdomain equations*

The substitution of the mode transformations described in equations (7.11) and (7.12) into the functional in equation (7.1) together with its variation $\delta H_{\mathrm{sf}} = 0$ allows us to obtain the following equations:

$$\tilde{\boldsymbol{M}}\ddot{\tilde{\boldsymbol{Q}}} + \tilde{\boldsymbol{K}}\tilde{\boldsymbol{Q}} = \tilde{\boldsymbol{R}}^{\mathrm{T}}\tilde{\boldsymbol{P}} + \tilde{\boldsymbol{F}}, \tag{7.13}$$

$$\tilde{\boldsymbol{m}}\ddot{\tilde{\boldsymbol{P}}} + \tilde{\boldsymbol{k}}\tilde{\boldsymbol{P}} = -\tilde{\boldsymbol{R}}\ddot{\tilde{\boldsymbol{Q}}} + \tilde{\boldsymbol{f}}, \tag{7.14}$$

where

$$\left.\begin{aligned} \tilde{\boldsymbol{M}} = \tilde{\boldsymbol{\Phi}}^{\mathrm{T}}\boldsymbol{M}\tilde{\boldsymbol{\Phi}}, \quad \tilde{\boldsymbol{K}} = \tilde{\boldsymbol{\Phi}}^{\mathrm{T}}\boldsymbol{K}\tilde{\boldsymbol{\Phi}}, \quad \tilde{\boldsymbol{F}} = \tilde{\boldsymbol{\Phi}}^{\mathrm{T}}\hat{\boldsymbol{F}}, \\ \tilde{\boldsymbol{m}} = \tilde{\boldsymbol{\varphi}}^{\mathrm{T}}\boldsymbol{m}\tilde{\boldsymbol{\varphi}}, \quad \tilde{\boldsymbol{k}} = \tilde{\boldsymbol{\varphi}}^{\mathrm{T}}\boldsymbol{k}\tilde{\boldsymbol{\varphi}}, \quad \tilde{\boldsymbol{f}} = \tilde{\boldsymbol{\varphi}}^{\mathrm{T}}\hat{\boldsymbol{f}}, \quad \tilde{\boldsymbol{R}} = \tilde{\boldsymbol{\varphi}}^{\mathrm{T}}\boldsymbol{R}\tilde{\boldsymbol{\Phi}}. \end{aligned}\right\} \tag{7.15}$$

The symmetrization of equations (7.13) and (7.14) has been discussed previously (see Xing & Price 1991), and the argument is not reiterated here.

8. Special techniques

(*a*) *Frequency shift*

In the previous discussion, the inverse matrices $(K^{ii})^{-1}$ in equation (4.11), $\boldsymbol{K}^{-1}$ in equation (5.6) and $(k^{ii})^{-1}$ in equation (6.5) are required for the proposed methods to be readily usable. However, if a matrix is singular difficulties arise. These can be overcome by application of a frequency shift technique which is now discussed.

(i) *Global eigenvalue problem*

Let us consider the eigenvalue problem

$$\boldsymbol{K}\boldsymbol{\Phi} = \zeta\boldsymbol{M}\boldsymbol{\Phi}. \tag{8.1}$$

Here ζ and $\boldsymbol{\Phi}$ represent the eigenvalue and the corresponding eigenvector. The adding of a term $\zeta_1 \boldsymbol{M}\boldsymbol{\Phi}$ to each side of equation (8.1) gives

$$\check{\boldsymbol{K}}\boldsymbol{\Phi} = \check{\zeta}\boldsymbol{M}\boldsymbol{\Phi}, \tag{8.2}$$

where

$$\check{\boldsymbol{K}} = \boldsymbol{K} + \zeta_1 \boldsymbol{M}, \tag{8.3}$$

$$\check{\zeta} = \zeta + \zeta_1, \tag{8.4}$$

and the additional quantity ζ_1 provides the means to cause a *frequency shift*. From a comparison of equations (8.1) and (8.2), we can conclude that the eigenvalue problem in equation (8.1) and the eigenvalue problem in equation (8.2) give the same eigenvector and the corresponding eigenvalue differ by a frequency shift ζ_1. Therefore, if the matrix $\boldsymbol{K}$ is singular, we obtain its solution by solving the eigenvalue problem in equation (8.2) with the non-singular matrix $\check{\boldsymbol{K}}$.

(ii) *Substructure or subdomain method*

To extend the discussion, let us assume that the equation describing the eigenvalue problem for substructure (α) is of the form

$$\boldsymbol{M}^{(\alpha)}\ddot{\boldsymbol{U}}^{(\alpha)} + \boldsymbol{K}^{(\alpha)}\boldsymbol{U}^{(\alpha)} = 0. \tag{8.5}$$

The appropriate equations after synthesis are described in equations (5.25), (5.29) and (5.30) with $\check{\boldsymbol{F}} = \boldsymbol{0}$. Now, if a frequency shift ζ_1 is given to each substructure (α), the corresponding equation describing the substructure is

$$\boldsymbol{M}^{(\alpha)}\ddot{\boldsymbol{U}}^{(\alpha)} + \check{\boldsymbol{K}}^{(\alpha)}\boldsymbol{U}^{(\alpha)} = 0, \tag{8.6}$$

where now

$$\check{\boldsymbol{K}}^{(\alpha)} = \boldsymbol{K}^{(\alpha)} + \zeta_1 \boldsymbol{M}^{(\alpha)}. \tag{8.7}$$

Based on this discussion it follows that equation (8.6) gives the same eigenvector $\boldsymbol{\Phi}^{(\alpha)}$ and an eigenvalue with a frequency shift ζ_1 as given by equation (8.5). The quantities $\check{\boldsymbol{\xi}}^{(\alpha)}$ and $\check{\boldsymbol{\Lambda}}^{(\alpha)}$ represent the consistent force modes and eigenvalue diagonal matrix of equation (8.6). Therefore, from equations (8.3), (8.4), (5.14) and (5.17) we obtain the following results:

$$\left.\begin{aligned} \check{\boldsymbol{\Lambda}}^{(\alpha)} &= \boldsymbol{\Lambda}^{(\alpha)} + \zeta_1 \boldsymbol{I}^{(\alpha)}, \quad \check{\boldsymbol{\Lambda}}_k^{(\alpha)} = \boldsymbol{\Lambda}_k^{(\alpha)} + \zeta_1 \boldsymbol{I}_k^{(\alpha)}, \\ \check{\boldsymbol{\Lambda}}_h^{(\alpha)} &= \boldsymbol{\Lambda}_h^{(\alpha)} + \zeta_1 \boldsymbol{I}_h^{(\alpha)}, \quad \check{\boldsymbol{\xi}}^{(\alpha)} = \boldsymbol{\Phi}_h^{(\alpha)} \check{\boldsymbol{\Lambda}}_h^{(\alpha)(-1)} \boldsymbol{\Phi}_h^{j(\alpha)\mathrm{T}}, \end{aligned}\right\} \tag{8.8}$$

and orthogonal relations

$$\check{\boldsymbol{\xi}}^{(\alpha)\mathrm{T}}\boldsymbol{M}^{(\alpha)}\boldsymbol{\Phi}^{(\alpha)} = 0, \quad \check{\boldsymbol{\xi}}^{(\alpha)\mathrm{T}}\boldsymbol{K}^{(\alpha)}\boldsymbol{\Phi}^{(\alpha)} = 0. \tag{8.9}$$

The corresponding mode transformation relation is

$$\boldsymbol{U}^{(\alpha)} = [\check{\boldsymbol{\xi}}^{(\alpha)} \quad \boldsymbol{\Phi}_k^{(\alpha)}] \begin{bmatrix} \mu^{j(\alpha)} \\ Q_k^{(\alpha)} \end{bmatrix} = \check{\boldsymbol{\Phi}}\tilde{\boldsymbol{Q}}, \tag{8.10}$$

and by using equations (8.8) and (8.9), we can transform equation (8.5) into the form,

$$\tilde{\boldsymbol{M}}^{(\alpha)}\ddot{\tilde{\boldsymbol{Q}}}^{(\alpha)} + \tilde{\boldsymbol{K}}^{(\alpha)}\tilde{\boldsymbol{Q}}^{(\alpha)} = 0, \tag{8.11}$$

where

$$\tilde{\boldsymbol{M}}^{(\alpha)} = \begin{bmatrix} \check{\boldsymbol{\xi}}^{(\alpha)\mathrm{T}} \boldsymbol{M}^{(\alpha)} \check{\boldsymbol{\xi}}^{(\alpha)} & 0 \\ 0 & \boldsymbol{I}_k^{(\alpha)} \end{bmatrix}, \tag{8.12}$$

$$\tilde{\boldsymbol{K}}^{(\alpha)} = \begin{bmatrix} \check{\boldsymbol{\xi}}^{(\alpha)\mathrm{T}} \boldsymbol{K}^{(\alpha)} \check{\boldsymbol{\xi}}^{(\alpha)} & 0 \\ 0 & \boldsymbol{\Lambda}_k^{(\alpha)} \end{bmatrix}. \tag{8.13}$$

Because the transformation in equation (8.9) is orthogonal, equation (8.11) has the same eigenvalue and same eigenvector space as belongs to equation (8.5). Furthermore, it follows by similar arguments to those described in the development of equations (5.23), (5.25), (5.29) and (5.30) but with $\check{\boldsymbol{\xi}}$ replacing $\boldsymbol{\xi}$ that the equivalent equation after synthesis of equations (8.11) is of the form,

$$\check{\boldsymbol{M}} \ddot{\check{\boldsymbol{Q}}} + \check{\boldsymbol{K}} \check{\boldsymbol{Q}} = \boldsymbol{0}. \tag{8.14}$$

This also has the same eigenvalue and eigenvector space as equation (5.29) with $\check{\boldsymbol{F}} = \boldsymbol{0}$.

On the other hand, the transformation (8.10) can transform equation (8.6) into the form,

$$\tilde{\boldsymbol{M}}^{(\alpha)} \ddot{\tilde{\boldsymbol{Q}}}^{(\alpha)} + \hat{\boldsymbol{K}}^{(\alpha)} \tilde{\boldsymbol{Q}}^{(\alpha)} = 0, \tag{8.15}$$

where

$$\hat{\boldsymbol{K}}^{(\alpha)} = \begin{bmatrix} \check{\boldsymbol{\xi}}^{(\alpha)\mathrm{T}} \check{\boldsymbol{K}}^{(\alpha)} \check{\boldsymbol{\xi}}^{(\alpha)} & 0 \\ 0 & \check{\boldsymbol{\Lambda}}_k^{(\alpha)} \end{bmatrix} \tag{8.16}$$

$$= \tilde{\boldsymbol{K}}^{(\alpha)} + \zeta_1 \tilde{\boldsymbol{M}}^{(\alpha)}. \tag{8.17}$$

It can be shown that the appropriate valid equation after synthesis of equation (8.15) is

$$\check{\boldsymbol{M}} \ddot{\check{\boldsymbol{Q}}} + (\check{\boldsymbol{K}} + \zeta_1 \check{\boldsymbol{M}}) \check{\boldsymbol{Q}} = \boldsymbol{0}. \tag{8.18}$$

This implies that equation (8.18) has the same eigenvector to equation (8.14) and an eigenvalue with a frequency shift ζ_1. Thus equation (8.18) also has the same eigenvector space and an eigenvalue with a frequency shift ζ_1 corresponding to equation (5.29) with $\check{\boldsymbol{F}} = \boldsymbol{0}$.

On the basis of this discussion, we conclude that a frequency shift technique can be used in the hybrid substructure displacement model to overcome the difficulty of singularity in matrix $\boldsymbol{K}$. For the consistent displacement model for the solid and the pressure equilibrium model for the fluid the same conclusion can also be reached. For the coupling fluid–solid case the conclusion may not be deduced because of symmetry reasons. However, if there is a fixed interface for each solid substructure with a wet interface, normally a singular matrix does not exist and there is no need to use the frequency shift technique. If, in the rare case, a singularity exists, modifications to the substructure idealization can usually overcome this problem.

(*b*) *Ground motion*

The prediction of the dynamical response of a system excited by ground motion, for example an earthquake, is a problem of great practical importance. To demonstrate how this problem can be discussed in the analytical framework created previously,

PHILOSOPHICAL TRANSACTIONS OF THE ROYAL SOCIETY A MATHEMATICAL, PHYSICAL & ENGINEERING SCIENCES

let us consider the coupling equations (7.2) and (7.3). These can be rewritten as

$$\boldsymbol{M}\ddot{\boldsymbol{U}} + \boldsymbol{K}\boldsymbol{U} = \boldsymbol{R}^{\mathrm{T}}\boldsymbol{p} + \hat{\boldsymbol{F}}, \tag{8.19}$$

$$\boldsymbol{m}\ddot{\boldsymbol{p}} + \boldsymbol{k}\boldsymbol{p} = -\boldsymbol{R}\ddot{\boldsymbol{U}} + \hat{\boldsymbol{f}}, \tag{8.20}$$

and there exists (for sake of argument) a ground motion $\hat{\boldsymbol{U}}$ and $\ddot{\hat{\boldsymbol{U}}}$ exciting this coupled system (that is, for example, in practical terms the fluid–structure interaction excited in a dam by an earthquake). The motion of the structure may be written as

$$\boldsymbol{U} = \hat{\boldsymbol{U}} + \tilde{\boldsymbol{U}}, \tag{8.21}$$

where $\tilde{\boldsymbol{U}}$ represents the motion of the structure relative to the ground. Substituting equation (8.21) into equations (8.19) and (8.20), we obtain equations

$$\boldsymbol{M}\ddot{\tilde{\boldsymbol{U}}} + \boldsymbol{K}\tilde{\boldsymbol{U}} = \boldsymbol{R}^{\mathrm{T}}\boldsymbol{p} + \hat{\boldsymbol{F}} - \boldsymbol{M}\ddot{\hat{\boldsymbol{U}}}, \tag{8.22}$$

$$\boldsymbol{m}\ddot{\boldsymbol{p}} + \boldsymbol{k}\boldsymbol{p} = -\boldsymbol{R}\ddot{\tilde{\boldsymbol{U}}} + \hat{\boldsymbol{f}} - \boldsymbol{R}\ddot{\hat{\boldsymbol{U}}}, \tag{8.23}$$

where the relation obtained from the rigid motion $\hat{\boldsymbol{U}}$ of structure

$$\boldsymbol{K}\hat{\boldsymbol{U}} = 0 \tag{8.24}$$

is used.

From equations (8.22) and (8.23), we find that the excitation of ground motion may be regarded as a force $-\boldsymbol{M}\ddot{\hat{\boldsymbol{U}}}$ added to the structure and a force $-\boldsymbol{R}\ddot{\hat{\boldsymbol{U}}}$ applied to the fluid.

9. Numerical examples

To complement the mixed finite-element substructure–subdomain method presented herein, a specialized computer algorithm (FSIAP92) based on PC architecture was developed to solve large dynamical response problems associated with structure, fluids and fluid–structure interactions. This user friendly software contains all the theoretical features discussed in the development of the approach and overcomes restrictions on computer storage capacity, length of run time, etc., providing an effective and efficient solution to complex fluid–structure dynamical interaction problems.

To provide an insight into the range of application of the theory and software, a selection of practical examples are discussed. Wherever possible, predictions from the proposed mathematical model are compared with results derived from analytical solutions, other software packages and other mathematical or theoretical models.

(*a*) *Eigenvalue and dynamical response analysis of a two-dimensional fluid container excited by a ground motion*

Figure 4 illustrates a two-dimensional fluid container (e.g. oil storage or water storage tank) with rigid boundaries of length $L = 160$ m and height $H = 160$ m. It is assumed excited by an earthquake creating an idealized horizontal ground motion $\ddot{U} = -\cos(2\pi ft)$ with a frequency of excitation $f = 3.0$ Hz. If the free surface wave is neglected, the theoretical solution of the natural frequencies of the water pond is

$$f_{mn} = \frac{\lambda_{mn}c}{2\pi} \qquad (n = 0, 1, 2, \ldots; \quad m = 1, 3, 5, \ldots), \tag{9.1}$$

Table 1. *A comparison of the calculated and theoretical natural frequencies* (Hz) *of the two-dimensional fluid container illustrated in figure 4*

mode number	calculation	theoretical
1	2.2488	2.223438
2	5.1062	4.996214
3	7.0940	6.703125
4	8.4464	8.056154
5	10.108	9.212564

where $c = 1430\,\mathrm{m\,s^{-1}}$ denotes the velocity of sound in water, and the dynamical pressure on the left wall excited by the ground motion is given by

$$p(0,y,t) = \frac{8\rho H}{\pi^2}\sum_{n=0}^{\infty}\frac{\lambda_n}{(2n+1)^2}\{\cos(2\pi ft)\frac{1-\cosh(kL)}{k\sinh(kL)} + \frac{4}{L}\sum_{m=1,3,5,\ldots}^{\infty}\frac{1}{\lambda_m^2+k^2}\cos(\lambda_{mn}ct)\}\sin(\lambda_n y), \tag{9.2}$$

where

$$\left.\begin{aligned}\lambda_n = (2n+1)\pi/2H \quad (n=0,1,2,\ldots), \qquad \lambda_m = m\pi/L \quad (m=1,3,5,\ldots),\\ k=\sqrt{\lambda_n^2-4\pi^2f^2/c^2}, \qquad \lambda_{mn}=\sqrt{\lambda_n^2+\lambda_m^2}.\end{aligned}\right\} \tag{9.3}$$

As shown in figure 4, 16 four-node two-dimensional isoparametric fluid pressure elements of equal size were used to discretize the enclosed fluid domain. At each node of each pressure element there is prescribed only one pressure variable so that 25 degrees of freedom are admitted in the analysis. For this model, the calculated first 5 eigenvalues are listed in table 1. The calculated dynamical pressure at point A on the left wall is illustrated and compared with the theoretical prediction (i.e. equation (9.2)). It is found that both calculations are in reasonable agreement with the theoretical results, even taking this relatively crude (simple) idealization.

(*b*) *Dynamic response of a two-dimensional dam–water system excited by a ground motion*

Figure 5 illustrates a two-dimensional dam–water system of the same dimensions as shown in the previous example (see figure 4). The dam is idealized as a uniform elastic structure of Young's modulus $E = 2.4\times10^9\,\mathrm{kg\,m^{-2}}$, Poisson ratio $\nu = 0.17$, and the system is again excited by a horizontal ground motion as defined previously. The dam is of width 120 m at base and 15 m at top. To predict the dynamical characteristics and responses of this water-dam system, as shown in figure 5, 16 four-node isoparametric fluid pressure elements (similar to the ones illustrated in figure 4) and eight four-node isoparametric solid plane strain elements were adopted to describe the fluid–structure interaction. Since to each node of a solid plane strain element there are prescribed two displacement degrees of freedom and to each node of a fluid pressure element there is attached one pressure variable, it follows that

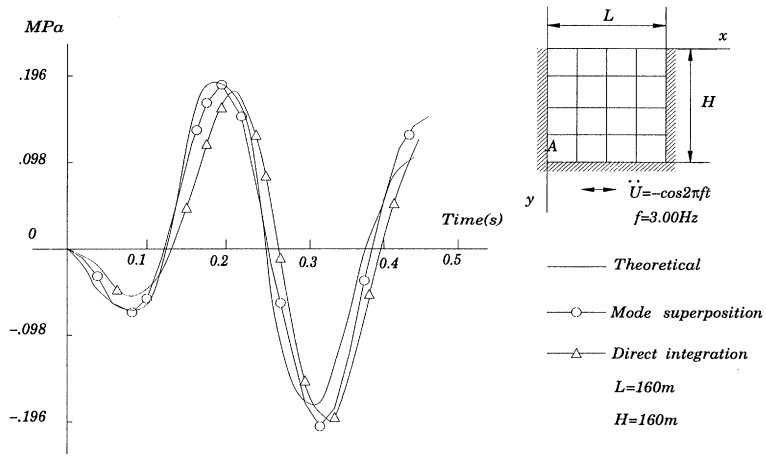

Figure 4. A 16 fluid pressure element idealization is used to calculate the dynamical characteristics of a two-dimensional square fluid container with rigid boundaries of length $L = 160$ m $= H$ excited by a ground motion $\ddot{U} = -\cos(2\pi ft)$, $f = 3.0$ Hz. Comparisons are presented of the dynamical pressure results at point A on the left wall derived from various prediction methods. That is, theoretical (——), numerical by a direct time integral approach with $\Delta t = 0.01S$ $(-\triangle-)$ and numerical by mode superposition using the first 16 mode $(-\circ-)$ solutions.

each node on the wet interface is associated with three degrees of freedom and the whole dynamic system is thus defined by 55 degrees of freedom (30 for displacement and 25 for pressure). In the numerical analysis, the first 16 modes of vibration are admitted in the calculation of the dynamic pressure at each fluid node and the displacement or stress at each node in the solid elements. The black line represents the theoretical solution of the dynamical pressure at the point A on the dam–water coupling interface if the dam is assumed rigid. The numerical solution by mode superposition is represented by the line $(-\circ-)$. When the elastic modulus is increased to $E = 2.4 \times 10^{11}$ kg m^{-2}, the calculated result is represented by the line $(-\triangle-)$ in figure 5. As expected, it is seen that the solution obtained for the dam modelled by the higher elastic modulus lies closer to the solution derived assuming a rigid dam. The influence of flexibility is readily demonstrated.

(*c*) *Dynamic response of a two-dimensional beam–water system excited by a pressure wave*

Figure 6 represents a two-dimensional beam–water system. The two-dimensional flexible beam is of height $H = 160$ m and the domain of water is of length $L = 1600$ m. The properties of this beam are as follows: gravity density of beam $\gamma_s = 2.0 \times 10^{-3}$ kg cm^{-3}, elastic modulus $E = 2.4 \times 10^5$ kg cm^{-2}, Poisson ratio $\nu = 0.3$, section area $B = 2.56 \times 10^6$ cm^2 and section moment of inertia $J = 5.461 \times 10^{11}$ cm^4. In this example the system is excited by a triangular pressure wave caused by an earthquake as shown in figure 7.

As illustrated in figure 6, this interactive solid-fluid system is modelled by 48 four-node isoparametric fluid pressure elements, four two-node beam elements and 65 nodes. In the mode superposition calculation, the first 20 modes of vibration are admitted into the analysis. Figure 8 shows the dynamical pressure curves at the points $y = 0$ m, 200 m, 600 m, 1000 m, and 1400 m along the horizontal line $z = 80$ m

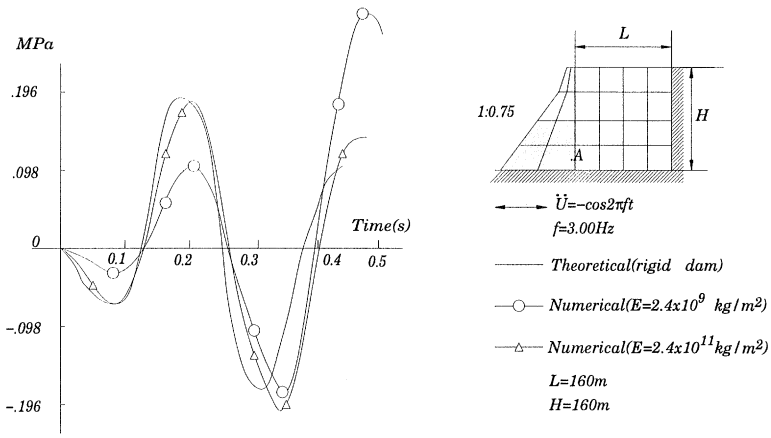

Figure 5. Sixteen fluid pressure elements and eight solid plane strain elements are used to calculate the dynamical responses of a two-dimensional dam–water system ($L = 160$ m $= H$) excited by a ground motion $\ddot{U} = -\cos(2\pi ft)$ with the frequency $f = 3.0$ Hz. The velocity of sound in water is $c = 1430\ \mathrm{m\,s^{-1}}$. The line $(-)$ represents the theoretical solution of the dynamical pressure at the point A on the dam–water coupling interface if the dam is assumed rigid. The numerical solution by mode superposition is represented by the line $(-\circ-)$ with Young's modulus $E = 2.4 \times 10^9\ \mathrm{kg\,m^{-2}}$. For an elastic modulus $E = 2.4 \times 10^{11}\ \mathrm{kg\,m^{-2}}$ and Poisson ratio $\nu = 0.17$, the calculated result is given by the line $(-\triangle-)$, which is in closer agreement to the prediction based on a rigid body assumption.

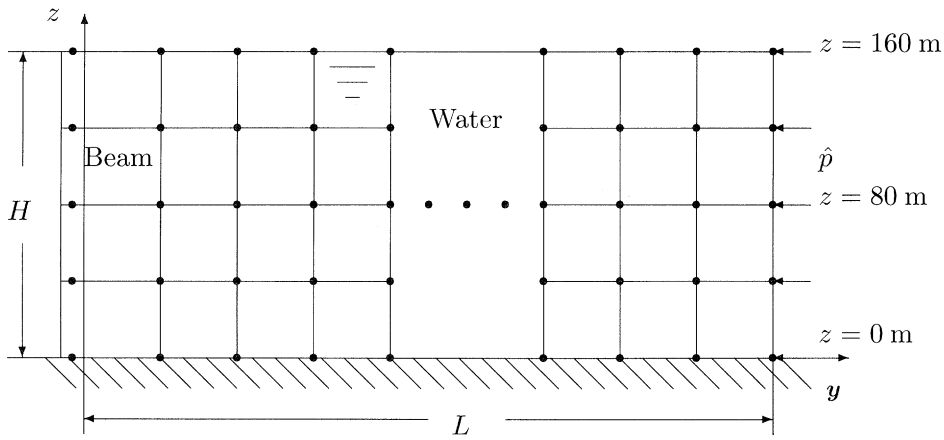

Figure 6. A finite-element idealization of a beam–water system consisting of four solid beam elements and 48 two-dimensional fluid pressure elements as well as 65 nodes.

in the water. From figure 8 the transmission of the pressure wave can be clearly seen, which agrees well with practical observation.

(*d*) *Dynamic response of a three-dimensional arch dam–water system excited by a explosion pressure*

Figure 9 illustrates schematically a finite-element idealization of an arched dam–water system of dimensions height $H = 100$ m, $B1 = 271$ m, $B2 = 791$ m, length $L = 520$ m containing water of depth $h = 90$ m. The dam is constructed of materials with properties: gravity density of dam $\gamma_s = 2.4 \times 10^{-3}\ \mathrm{kg\,cm^{-3}}$, elastic modulus

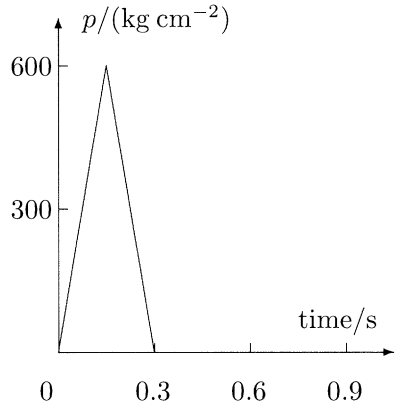

Figure 7. A triangle pressure wave excitation applied to the beam–water system in figure 6.

Table 2. *A comparison of natural frequencies* (Hz) *for structure shown in figure 12*

mode number	theory	FSIAP92	NASTRAN
1	0.00	0.00	0.00
2	0.85	0.61	0.61
3	2.03	1.74	1.73
4	3.70	3.33	3.32
5	5.84	5.38	5.37
6	8.46	7.89	7.88
7	11.56	10.85	10.85
8	15.13	14.27	14.28
9	19.13	18.11	18.18
10	23.72	22.37	22.55

$E = 2.4 \times 10^5$ kg cm^{-2} and Poisson ratio $\nu = 0.3$. To calculate the dynamical effect on the dam due to a centrally positioned explosion on the bottom of the reservoir, i.e. at position $L1 = 205$ m, $B3 = 249$ m as shown in figure 9, we idealized this system by 13 8–21-node three-dimensional isoparametric solid elements and 117 8–21-node three-dimensional isoparametric fluid pressure elements in addition to 289 nodes used to model the fluid–structure interaction. For simplification only, it is assumed that the infinite fluid domain can be suitably approximated by a finite domain and the fluid at great distances from the explosion remains undisturbed. These assumptions do not detract from the proposed mixed finite-element substructure–subdomain approach but they allow us to remain focused on the fluid–structure interaction in a simple way. Perhaps in this example, a more reasonable theoretical approach, though not necessary a more practical approach, would be to adopt infinite elements (see, for example, Zienkiewicz 1977) for the idealization of the fluid domain. This would enhance the overall solution process but introduce an extra spe-

PHILOSOPHICAL TRANSACTIONS OF THE ROYAL SOCIETY A MATHEMATICAL, PHYSICAL & ENGINEERING SCIENCES

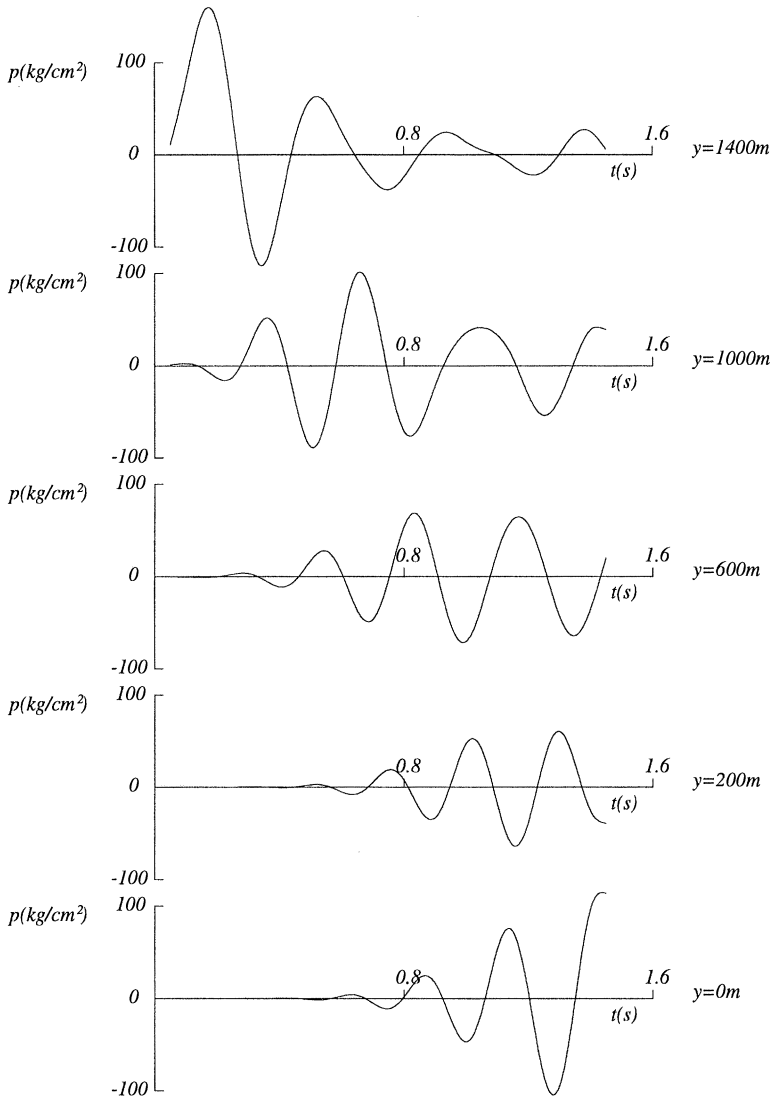

Figure 8. The dynamical pressure curves calculated at the points $y = 0$ m, 200 m, 600 m, 1000 m and 1400 m along the horizontal line $z = 80$ m in the fluid of the beam–water system in figure 6. This system is excited by the triangular pressure wave shown in figure 7.

cialization without adding significantly to the rigorous theoretical development of the subdomain-substructure approach, which is the principal theme of this paper.

In this example, the first 50 modes of vibration are used to calculate the dynamic responses by the mode superposition approach. Figure 10 illustrates the assumed pressure time history of the explosion. Figure 11*a* shows the displacement response in the z-direction at point A at the top of the arched dam and figure 11*b* illustrates the dynamical pressure at point B on the dam. Predicted values of responses at any node in the structure and fluid can be easily derived from such calculations.

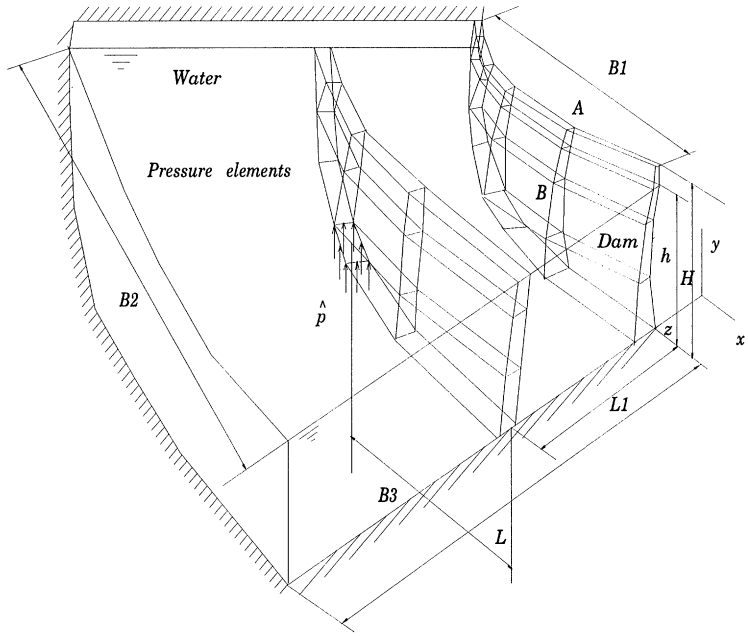

Figure 9. A sketch of a finite-element idealization of an arched dam–water system of $H = 100$ m, $B1 = 271$ m, $B2 = 791$ m, $L = 520$ m and water of depth $h = 90$ m. This model consists of 13 three-dimensional solid elements, 117 three-dimensional fluid pressure elements as well as 289 nodes. The centre of the explosion is located at the point $L1 = 205$ m and $B3 = 249$ m on the bottom of the reservoir. The pressure explosion characteristics are illustrated in figure 10.

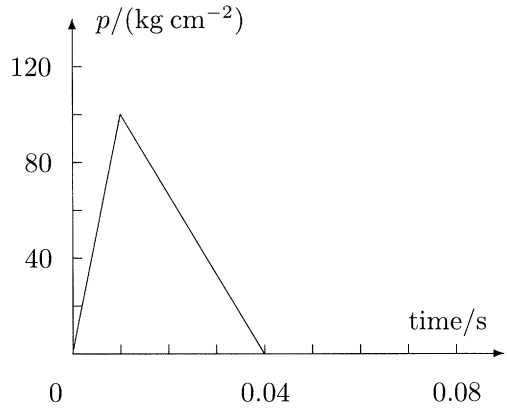

Figure 10. A triangle explosion pressure excitation applied at the bottom of the reservoir as shown in figure 9.

(*e*) *Prediction of structural-borne noise*

The developed theory is also suitable to analyse acoustic-structure interaction as well as fluid–structure interaction and the example in figure 12 shows a finite-element idealization of a section of fuselage as previously investigated by Sengupta *et al.* (1986). The properties of this fuselage section chosen by these authors are as

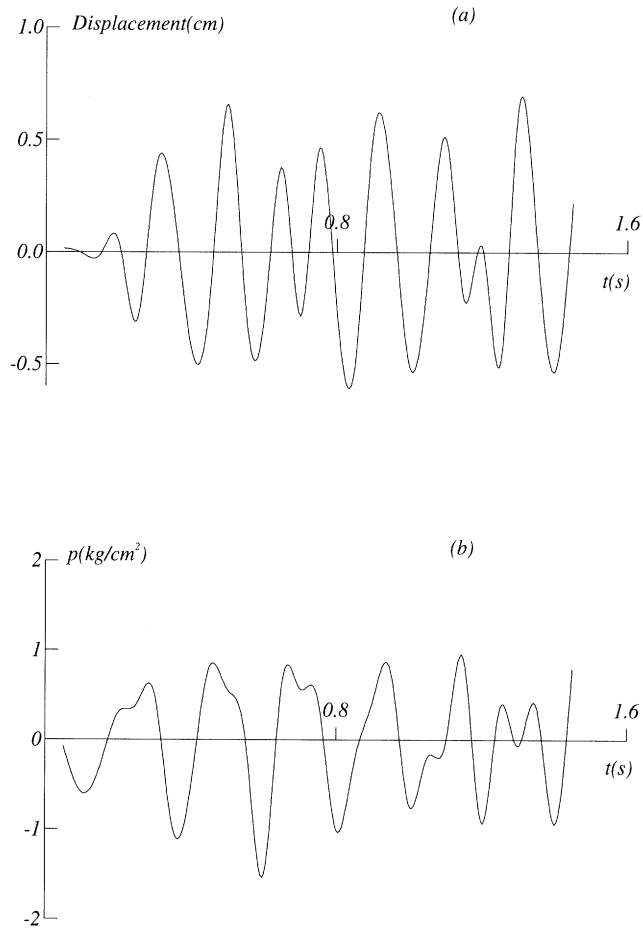

Figure 11. (*a*) The displacement response at point A in the z-direction on the top of the arched dam shown in figure 9; (*b*) the dynamical pressure at point B.

follows: its radius $R = 91.44$ cm, wall thickness $t = 0.08128$ cm, thickness along the longitudinal z-direction $B = 2.54$ cm, velocity of sound in air $c = 3.40 \times 10^4 c\ \mathrm{m\ s^{-1}}$, density of gravity of air $\gamma_\mathrm{a} = 1.22513 \times 10^{-6}\ \mathrm{kg\ cm^{-3}}$, gravity density of structure $\gamma_\mathrm{s} = 2.79454 \times 10^{-3}\ \mathrm{kg\ cm^{-3}}$, elastic modulus $E = 7.38231 \times 10^6\ \mathrm{kg\ cm^{-2}}$, the Poisson ratio $\nu = 0.3$, and excitation force $F = F_0 \mathrm{e}^{\mathrm{i}\omega t}$ with $F_0 = 2.2246$ N.

In the mode superposition approach, the structure was idealized by 20 beam elements, the air acoustic volume modelled by 160 two-dimensional isoparametric fluid pressure elements and 40 modes of vibration were admitted in the prediction of the dynamic responses. The frequencies of the flexible structure and the acoustic frequencies of the cavity assuming a rigid wall calculated by FSIAP92 are listed in table 2 and table 3. These are compared with the results calculated by NASTRAN and a theoretical solution given by Sengupta *et al.* The frequencies associated with the coupled air–structure interaction calculated by FSIAP92 are listed in table 4 which is additional to previous results. Apart from the first mode which is a constant pressure

Table 3. *Natural frequencies* (Hz) *of the sound volume with rigid wall as shown in figure 12*

mode number	theory	FSIAP92	NASTRAN
1	000.00	000.00	000.00
2	109.01	109.33	109.80
3	180.83	181.74	180.07
4	226.86	228.84	224.65
5	248.74	250.96	246.09
6	314.82	319.51	308.92
7	315.64	320.28	313.41
8	379.83	388.50	368.97
9	397.04	404.12	392.53
10	415.36	426.86	401.22

Table 4. *Natural frequencies* (Hz) *of the coupled structural-borne noise in the fuselage section as shown in figure 12 calculated by FSIAP92*

mode no.	frequency	mode no.	frequency	mode no.	frequency
1	0.0000	11	22.691	21	219.62
2	0.1327	12	27.701	22	290.83
3	0.4730	13	32.866	23	326.78
4	1.2303	14	38.063	24	359.05
5	2.4744	15	43.029	25	409.83
6	4.3636	16	47.542	26	425.40
7	6.8460	17	51.280	27	484.17
8	10.034	18	53.994	28	497.67
9	13.756	19	55.478	29	526.05
10	18.026	20	140.31	30	559.58

mode with zero frequency the first seven natural modes of the sound volume with a rigid wall are shown in figure 13. The natural modes of the structure are shown in figure 14 and the coupling modes are displayed in figure 15. The displacement response, due to a sinusoidal excitation with different frequencies, at the point A on the wall of the fuselage and the sound pressure level at points A, B and C in the sound cavity are given in figures 16 and 17 respectively. These curves also illustrate a comparison between the present calculation using FSIAP92 and NASTRAN used by Sengupta *et al.* Good agreement is found between these predictions which have been derived by alternative methods.

10. Conclusion

Several substructure–subdomain methods are presented to describe the dynamical behaviour of solids, fluids and fluid–structure interactions. A displacement consis-

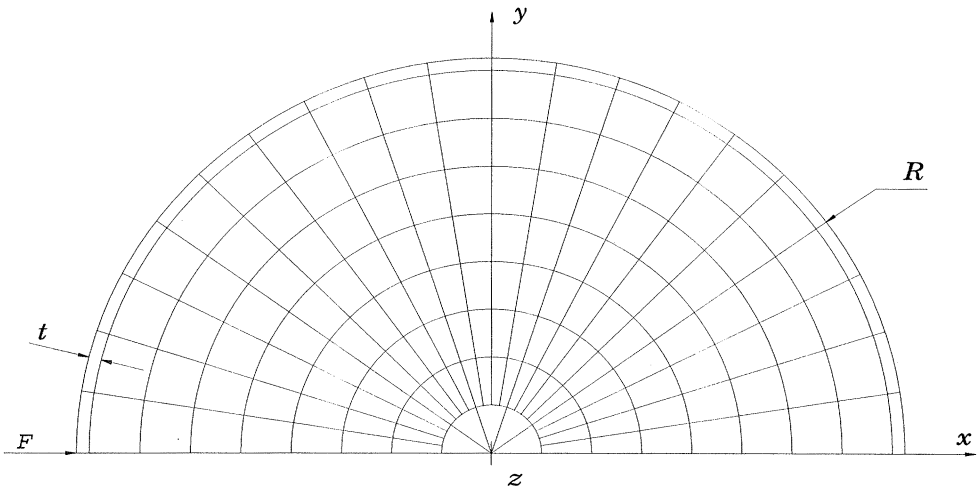

Figure 12. A finite-element idealization of a two-dimensional sound volume of a typical half section of a fuselage. The radius of this section $R = 91.44$ cm, the wall thickness $t = 0.08128$ cm, the thickness along the longitudinal z-direction $B = 2.54$ cm, the velocity of sound in air $c = 3.40 \times 10^4$ cm s^{-1}, the density of gravity of air $\gamma_a = 1.22513 \times 10^{-6}$ kg cm^{-3}, the gravity density of structure $\gamma_s = 2.79454 \times 10^{-3}$ kg cm^{-3}, the elastic modulus $E = 7.38231 \times 10^6$ kg cm^{-2}, the Poisson ratio $\nu = 0.3$, the excitation force $F = F_0 e^{i\omega t}$, $F_0 = 2.2246$ N.

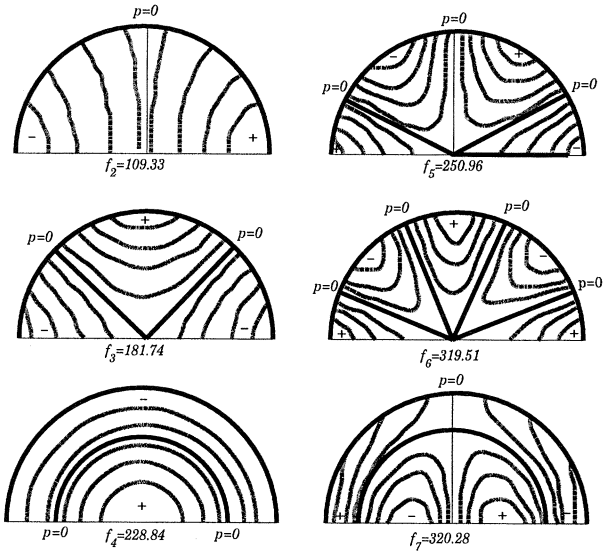

Figure 13. Natural modes of the sound volume assuming a rigid wall as shown in figure 12.

tency model and a hybrid displacement model for solid substructure, a pressure equilibrium model for fluid subdomain as well as a mixed substructure–subdomain model for fluid–solid interacting systems are fully formulated. These methods are based on a variational approach in which the chosen arguments of the functional are the acceleration of solid and the pressure in the fluid. By this means a unified theory is developed in a logical manner and reasoned approximations introduced into

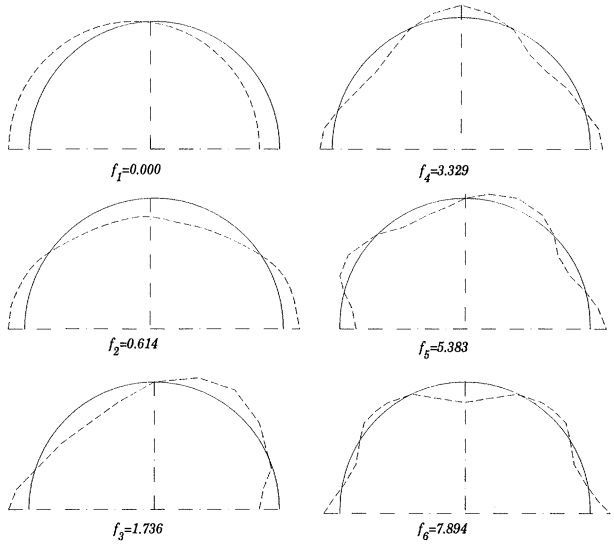

Figure 14. Natural modes of the structure without air coupling as shown in figure 12.

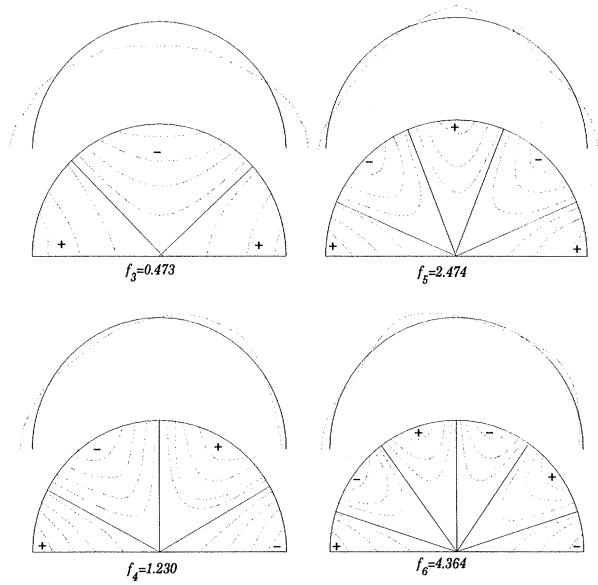

Figure 15. Natural modes of coupling structural-borne noise in the volume as shown in figure 12.

the analysis improving efficiency of computation without significantly deteriorating the accuracy of solution. The key to these achievements lies (i) in the selection of mode vectors and the rule for mode reduction and (ii) the synthesis of the equations modelling the dynamic interactions. The former allows the reduction in the number of degrees of freedom adopted in the full dynamic model describing the complex engineering system to a manageable size and hence eliminates the original necessity

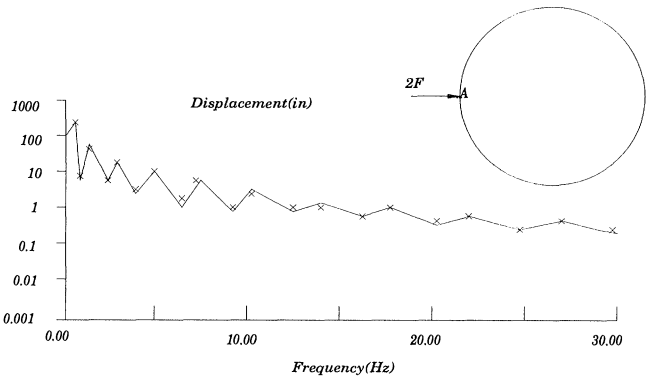

Figure 16. The variation of displacement response with excitation frequency at the point A on the structure. The black line (−) represents the solution by NASTRAN derived by Sengupta *et al.* (1986) and the points (×) denote solutions by FSIAP92.

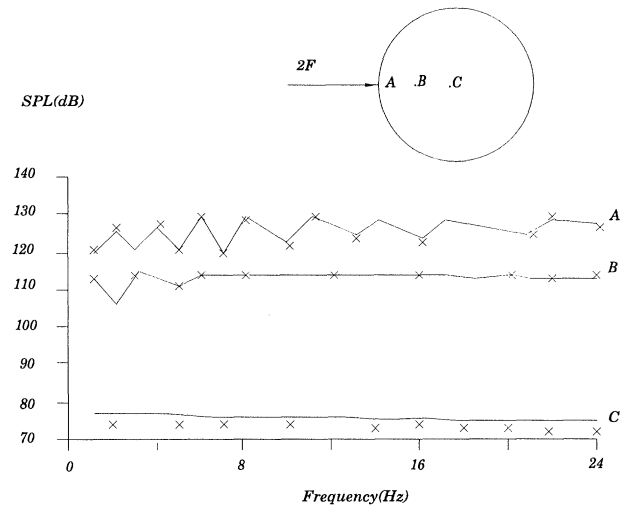

Figure 17. The variation of sound pressure responses with excitation frequency at the points A, B, and C in the air sound volume. The black line (−) represents the solution by NASTRAN given by Sengupta *et al.* (1986) and the points (×) denotes solutions by FSIAP92.

of using a large computer, whereas, the latter allows the transformation of the equations into matrix forms readily usable in suitably developed numerical schemes of analysis.

The success of the described theoretical approaches is demonstrated in the analysis of a range of fluid–structure and structural-airborne noise interacting systems. The comparisons of prediction of responses with analytical results and methods adopting alternative numerical approaches (e.g. NASTRAN) show good agreement. The mathematical models developed are readily adaptable for operation on PCs and workstations using purposely written software (FSIAP92). This greatly enhances the efficiency and effectiveness of the substructure–subdomain approaches to describe the dynamical behaviour of complex fluid–structure interacting systems.

We gratefully acknowledge the Royal Society for providing financial support enabling J.-T.X. to visit the University of Southampton. J.-T.X. expresses his deep appreciation to the National Education Commission of China and CAE for supporting the related research through the Doctorate Training Fund and the Science Foundation of Aeronautics and Astronautics.

References

Bishop, R. E. D. & Johnson, D. C. 1977 *The mechanics of vibration.* London: Cambridge University Press.

Craig, R. R. & Chang, C. J. 1977 On the use of attachment modes in substructure coupling for dynamical analysis. Paper 77-405. *AIAA/ASME 18th Struct. Dyn. and Mater. Conf., San Diego.*

Craig, R. R. & Bampton, M. C. C. 1968 Coupling of substructures for dynamical analysis. *AIAA Jl* **6**, 1313–1319.

Hou, S. N. 1969 Review of modal synthesis techniques and a new approach. *Shock Vib. Bull.* **40**, 25–29. (US Naval Research Laboratory.)

Hunn, B. A. 1955 A method of calculating normal modes of an aircraft. *Q. Jl Mech. Appl. Math.* **8**, 38–58.

Hurty, W. C. 1960 Vibration of structural systems by component mode synthesis. *ASME Jl Engng Mech. Div.* **85**, 51–69.

Hurty, W. C. 1965 Dynamic analysis of structural systems using component modes. *AIAA Jl* **3**, 678–685.

MacNeal, R. H. 1977 A hybrid method of component mode synthesis. *Computers Struct.* **1**, 581–601.

Rubin, S. 1975 Improved component-mode representation for structural dynamic analysis. *AIAA Jl* **13**, 995–1006.

Sengupta, G., Landann, A. E., Mera, A. & Yantis, T. F. 1986 Prediction of structure-borne noise, based on the finite element method. AIAA-86-1861, The Boeing Co., Seattle, WA.

Unruh, J. F. 1979 A finite-element sub-volume technique for structure-borne interior noise prediction. *AIAA 79-585 5th Aero. Acous. Conf., Seattle, WA.*

Wang, W.-L. 1979 A short review on mode synthesis technique and a new improvement. *Acta Aero. Astr. Sin.* **3**, 321–329. (In Chinese.)

Xing, J.-T. 1981 Variational principles for elastodynamics and study upon the theory of mode synthesis methods. Master thesis, Department of Engineering Mechanics, Qinghua University, Beijing, People's Republic of China. (In Chinese.)

Xing, J.-T. 1984 Some theoretical and computational aspects of finite element method and substructure–subdomain technique for dynamic analysis of the coupled fluid–solid interaction problems–variational principles for elastodynamics and linear theory of micropolar elasticity with their applications to dynamic analysis. Ph.D. dissertation, Department of Engineering Mechanics, Qinghua University, Beijing, People's Republic of China. (In Chinese.)

Xing, J.-T. 1986*a* A study on finite element method and substructure–subdomain technique for dynamic analysis of coupled fluid–solid interaction problems. *Acta Mech. Solida Sin.* **4**, 329–337. (In Chinese.)

Xing, J.-T. 1986*b* Mode synthesis method with displacement compatibility for dynamic analysis of fluid–solid interaction problems. *Acta Aero. Astr. Sin.* **7**, 148–156. (In Chinese.)

Xing, J.-T. & Price, W. G. 1991 A mixed finite element method for the dynamic analysis of coupled fluid–solid interaction problems. *Proc. R. Soc. Lond.* A **433**, 235–255.

Xing, J.-T. & Zheng, Z. C. 1983 A study upon mode synthesis methods based on variational principles for elastodynamics. *Acta Mech. Solida Sin.* **2**, 250–257. (In Chinese.)

Zienkiewicz, O. C. 1977 *The finite element method*, 3rd edn. London: McGraw-Hill.

Received 26 July 1994; revised 14 March 1995; accepted 4 May 1995

PHILOSOPHICAL TRANSACTIONS OF THE ROYAL SOCIETY A MATHEMATICAL, PHYSICAL & ENGINEERING SCIENCES